



The Hebrew University of Jerusalem
The Racah Institute of Physics

The surviving remnants of red giants after a partial tidal disruption event

השרידים של ענקים אדומים לאחר
אירוע קריעה גאותי חלקי

Núria Navarro

Thesis submitted in partial fulfillment of the requirements
for the Master of Sciences degree in Physics

Under the supervision of **Prof. Tsvi Piran**

November 2023



האוניברסיטה העברית בירושלים
מכון רקח לפיסיקה

The surviving remnants of red giants after a partial tidal disruption event

השרידים של ענקים אדומים לאחר
אירוע קריעה גאותי חלקי

מוגש על ידי
נוריה נווארו

עבודה זו הונחתה על ידי עבודת גמר לתואר מוסמך בפיסיקה

פרופ' צבי פירן

נובמבר 2023



The Hebrew University of Jerusalem
The Racah Institute of Physics

The surviving remnants of red giants after a partial tidal disruption event

Núria Navarro

Thesis submitted in partial fulfillment of the requirements
for the Master of Sciences degree

Under the supervision of **Tsvi Piran**

Signature of student: _____

Date: _____

Signature of supervisor: _____

Date: _____

Signature of chairperson of the
committee for graduate studies: _____

Date: _____

November 2023

תקציר

כאשר כוכב עובר ליד חור שחור ענקי הוא עלול להקרע על ידי כח הגאות של החור השחור, בתהליך הנקרא "אירוע קריעה גאותי" (Tidal Disruption Event). חלק משמעותי מאירועי קריעה גאותיים קורה לענקים אדומים. ענקים אדומים מאופיינים במבנה פנימי של ליבה דחוסה ומעטפת גדולה ודלילה, ההבדל המשמעותי בצפיפות בין שני החלקים הללו הופך אותם לאידיאלים עבור אירועי קריעה גאותיים חלקיים (Partial Tidal Disruption Event, PTDE), שבהם חלק מהכוכב מצליח לשרוד תהליך זה בלי להקרע. המחקר שלנו מתמקד בהתפתחות ארוכת הטווח של הענקים האדומים אשר עברו PTDE, באמצעות MESA, תוכנה אשר מבצעת סימולציית התפתחות כוכבים. תהליכי PTDE צפויים לקלף רק חלק יחסי מהחלק החיצוני של המעטפת של הענקים האדומים, מה שיותר כוכבים מקולפים בעלי תכונות מיוחדות, למשל, ליבה יותר גדולה ודחוסה, ומעטפת שהיא פחות צפופה. למרות שמסתם פחתה, לכוכבים מקולפים רדיוס דומה ובהירות מעט יותר גבוהה מאשר לכוכבים המקוריים. ההבדל בזמן החיים בין כוכבים רגילים ומקולפים מרמז על כך שענקים אדומים בעלי מסות נמוכות יכולים להיות שאריות של אירועי PTDE.

Abstract

When the orbit of a star gets close enough to a black hole, the star can get completely or partially torn apart by the tidal forces. A considerable amount of tidal disruption events (TDE) are of red giants. The internal structure of red giants consists of a very dense core and a large, low-density envelope. The sharp difference in density between these two regions makes them ideal candidates for a partial tidal disruption event (PTDE) with a surviving remnant. The main focus of our study is the long-term evolution of the surviving red giant victims of partial tidal disruption events using the MESA stellar evolution code. PTDEs are expected to peel off only a fraction of the outer layers of the red giant's envelope mass, resulting in stripped stars with distinct characteristics, including a more massive, denser core and a more tenuous envelope. Despite mass reduction, stripped stars maintain a similar radius and exhibit slightly higher luminosities. The difference in lifetime between the evolutionary tracks of normal and stripped stars suggests that low-mass red giants could be the remnants of PTDEs.

Acknowledgements

First and foremost, I would like to express my gratitude to Prof. Tsvi Piran, my advisor, for his guidance, dedication, and constant availability throughout the course of this project. Not only has he been supportive every step of the way, but he has also actively facilitated opportunities for my future academic growth.

I would like to extend my sincere appreciation to the astrophysics department at HUJI. Prof. Nicholas Stone deserves special thanks for his excellent course in stellar structure and evolution, patiently addressing every doubt with meticulous detail. Prof. Sivan Ginzburg, thank you for introducing me to MESA and answering my doubts. Dr. Matteo Pais has been the best office buddy, assisting me with the cluster and helping me improve my Italian, brewing delightful moka coffee, and consistently being there for me. Barak Rom, thank you for explaining me TDE rates. To my fellow master students —Maya, Ofek, Dina, Nadav, Oshri, and Racheli— your constant emotional support has meant the world to me.

I am deeply grateful to Prof. Selma de Mink for her support, encouragement, and for inviting me to the Max Planck Institute for Astrophysics. The time spent there allowed me to engage in insightful discussions about MESA, stellar evolution and academic careers. Heartfelt thanks to Rob Farmer, Prof. Mathieu Renzo, Prof. Alison Sills, Dr. Ylva Götberg, Dr. Taeho Ryu, Prof. Carles Badenes, Prof. Jim Fuller, Prof. Stephen Justham, and Dr. Evan Bauer for their invaluable comments, MESA explanations and insights on the project. Although the prospect of being at the MPA initially felt daunting, Aldana Grichener, Ruggero Valli, Rachel Patton, and

Aakash Bhat made me feel warmly welcomed.

Finally, special thanks to my partner, Yogev Hendel, for his priceless help with coding and data processing. Thanks to both Yogev and our friend Shai Keidar, for providing me with incredible meals during times when I was too busy to look after myself and for being the best people I have in my life.

Contents

List of Figures	vii
1 Introduction	1
2 Stellar evolution	3
2.1 Main sequence	3
2.1.1 Low mass stars - radiative cores	4
2.1.2 Intermediate mass stars - convective cores	5
2.2 Red giant phase	7
2.2.1 Low mass stars	7
2.2.2 Intermediate mass stars	9
2.3 Asymptotic giant branch	9
3 Tidal disruption events	12
3.1 Tidal radius	12
3.2 Partial TDEs	13
3.3 PTDEs of Red Giants	14
3.4 Rates	16
4 Methodology	18

<i>CONTENTS</i>	vi
4.1 MESA	18
4.2 Resolution tests	19
4.3 Simulating stripped stars	20
5 Results	22
5.1 Star profiles before and after stripping	25
5.2 Long-term evolution	31
5.2.1 Progenitor mass comparison	33
5.2.2 Total mass comparison	36
5.2.3 Stripping time comparison	39
6 Conclusion	41
7 Bibliography	43
A Table of all simulations	47
B Figures and tables of Section 5	50
B.1 Progenitor mass comparison	50
B.2 Total mass comparison	54
B.3 Stripping time comparison	57

List of Figures

2.1	HR diagram track of a $1 M_{\odot}$, $1 Z_{\odot}$ star	5
2.2	HR diagram tracks of $0.7 M_{\odot}$, $1 M_{\odot}$, $1.5 M_{\odot}$, $2 M_{\odot}$, $3 M_{\odot}$ stars with 0.1 Z_{\odot} metallicity	6
2.3	Density profile of $1 M_{\odot}$ and $2 M_{\odot}$ stars in the MS and RG	8
2.4	Radius vs time for $1 M_{\odot}$, $1.5 M_{\odot}$, $2 M_{\odot}$ and $3 M_{\odot}$, $0.1 Z_{\odot}$ stars . . .	10
2.5	Kippenhahn diagrams of normal stars	11
3.1	Tidal radius for stripped mass fraction for different stars masses . . .	15
3.2	Tidal radius for stripped mass fraction for different black hole masses	16
4.1	HR diagram of temporal and spatial resolution tests	20
5.1	Radius vs time of the RG phase with stripping points	23
5.2	Density profile of stars at 0.25 helium fraction.	24
5.3	Density profile of stars at 0.50 helium fraction.	24
5.4	Density profile of stars at 0.75 helium fraction.	25
5.5	Density and radius profiles for a $1 M_{\odot}$ star	27
5.6	Density and radius profiles for a $1.5 M_{\odot}$ star	28
5.7	Density and radius profiles for a $2 M_{\odot}$ star	29
5.8	Density and radius profiles for a $3 M_{\odot}$ star	30

5.9	Simulations in parameter space	31
5.10	Kippenhahn diagrams of stripped stars	32
5.11	Progenitor star and stripped stars comparison in parameter space . . .	33
5.12	Radius with time for progenitor and stars stripped at 0.50 helium fraction	34
5.13	Stars with same total mass comparison in parameter space	36
5.14	HR diagram tracks for $0.7 M_{\odot}$ stars, normal and stripped	37
5.15	Radius with time for stars with same total mass	38
5.16	Stars stripped at different times comparison in parameter space	39
5.17	Radius with time for stars stripped at different times	40
B.1	HR diagram tracks for progenitor and stripped stars comparison	53
B.2	HR diagram tracks for stripped/non-stripped comparison	56
B.3	HR diagram tracks for a stripping time comparison	59

1 Introduction

Tidal Disruption Events (TDE) have become an active subject of research in the past years. These phenomena usually occur in the context of dense environments, such as active galactic nuclei (AGN) or star clusters, where we can expect a great number of dynamical interactions between stars and compact objects. In particular, when the orbit of a star gets close enough to a black hole (BH), the star can get partially or completely torn apart by the tidal forces. As a result, a fraction of the mass falls onto the black hole, leading to a luminous flare that can be detected, and the remaining debris can become unbound or be accreted back onto the black hole. The observable signature of a TDE is regarded as an important tool to gather data on BH properties, the physics of accretion and jets.

A lot of research has been done on the hydrodynamics of the disruption of main sequence (MS) stars, as well as on the observable quantities of their resulting bright flares (see [Rossi et al. \(2021\)](#) for a review), but the disruption of red giant stars has been little explored. However, we expect that a considerable amount of TDEs are in fact of red giants. Firstly, the internal structure of red giants consists of a very dense core and a large, low-density envelope that can be easily removed. More interestingly, the sharp difference in density between these two regions makes them ideal candidates for a partial tidal disruption event (PTDE) with a surviving remnant. Secondly, red giants have radii that can be orders of magnitude bigger than their previous MS radius. Since the tidal radius depends linearly on the radius of the star, giant stars can be disrupted by the tidal forces at larger pericenter distances. Therefore, even though the lifetime of the giant phases of stellar evolution is shorter

than the MS lifetime, these two factors make giant stars a relevant contribution to all tidal disruption events.

Red giants are very likely to survive the encounter. The outer layers of the envelope can easily be peeled off while the compact core remains effectively unperturbed. This is the case for partial tidal disruptions, for which the remaining stars can become unbound and continue with their lives peacefully. A natural question arises: what will the long-term evolution of the surviving red giant stars look like? Can we spot any significant differences between their natural and perturbed evolutionary tracks in the HR diagram?

This is of special interest in the context of globular clusters, where the alleged presence of intermediate black holes would lead us to expect a high number of PTDEs and therefore, of remnant victim stars. As a result, we would have a presence of a population of unexpected stars. Therefore, the presence of such stars may indicate the presence of intermediate black holes.

With this motivation, the main focus of our study is the long-term evolution of the surviving red giant victims of PTDEs, exploring a wide range of different star masses, stripping times and stripped mass fraction. The structure of this work is as follows. In chapter 2, we present a short and qualitative description of stellar evolution, focusing on low and intermediate mass stars. In chapter 3, we introduce the basics of tidal disruption events, reviewing some well-understood order-of-magnitude derivations and the partial tidal disruption of red giants. In chapter 4 we describe the methodology, approximations and simulations with MESA. In chapter 5 we present and discuss our results.

2 Stellar evolution

In this chapter we will briefly review stellar evolution for low and intermediate mass stars ($0.8 M_{\odot} - 3 M_{\odot}$), based on [Kippenhahn et al. \(2012\)](#); [Hansen et al. \(2004\)](#).

When a star is in hydrostatic equilibrium (HSE), the inward pull of gravity is balanced by the outward push of gas and radiation pressure.

$$\frac{dP}{dr} = -\rho \frac{GM(r)}{r^2} \quad (2.1)$$

All the evolutionary stages are characterized by the ongoing interplay between these two forces and the continuous readjustment of the star to recover and maintain HSE.

2.1 Main sequence

The main sequence constitutes the longest stage of the lives of stars: it lasts $\sim 1 \times 10^{10}$ yr for solar-type stars. During this stage, gravity is balanced by the gas pressure thanks to the fusion of hydrogen (${}^1\text{H}$) into helium (${}^4\text{He}$), either by the proton-proton chain (if the mass of the star is $M_{\star} \lesssim 1.3 M_{\odot}$) or the CNO cycle (for $M_{\star} \gtrsim 1.3 M_{\odot}$). The latter is more sensitive to temperature, so it distributes energy production in a smaller region of the star, causing the core to be convective (as can be seen in the first panel of figures [2.5b](#), [2.5c](#) and [2.5d](#)). Stars with masses lower than $1.3 M_{\odot}$ fuse hydrogen through the pp-chain, which has a smaller sensitivity to temperature, energy production is distributed in a larger region and as a result the core is radiative (seen in first panel of figure [2.5a](#)).

The same threshold is found for energy transport in the envelope: stars of lower masses have neutral hydrogen, which raises the opacity and causes convection to take over. Stars of higher masses are hotter and thus hydrogen is mostly ionized, so energy is transported through radiation. Stars of about $0.3 M_{\odot}$ and below are fully convective, but they're out of the scope of this study.

As stars burn hydrogen during the main sequence, the molecular weight increases

$$\mu^{-1} = 2X + \frac{3}{4}Y + \frac{1}{2} \quad (2.2)$$

(where X is the H fraction and Y is the He fraction) and helium falls to the center.

As the chemical composition of the core changes, pressure decreases

$$P = \frac{\rho k T}{\mu m_{\text{H}}} \quad (2.3)$$

The core contracts until the density and temperature have increased enough to balance the inward pull of gravity. As a result, the fusion rate also increases and stars move towards higher luminosities during their main sequence.

The stellar evolution track will look somewhat different (as shown in figure 2.2) depending on whether there is mixing or not.

2.1.1 Low mass stars - radiative cores

Stars with mass $\lesssim 1.3 M_{\odot}$, with radiative cores, will develop an inhomogeneous structure over time: a growing, isothermal core of inert helium surrounded by a layer of hydrogen. The stellar evolution track in the HR diagram bends slightly to the left (see 2.1), since both luminosity and effective temperature increase. Once the core is depleted of hydrogen and develops the inhomogeneous structure, the fusion of hydrogen is shifted from the center of the core to a shell.

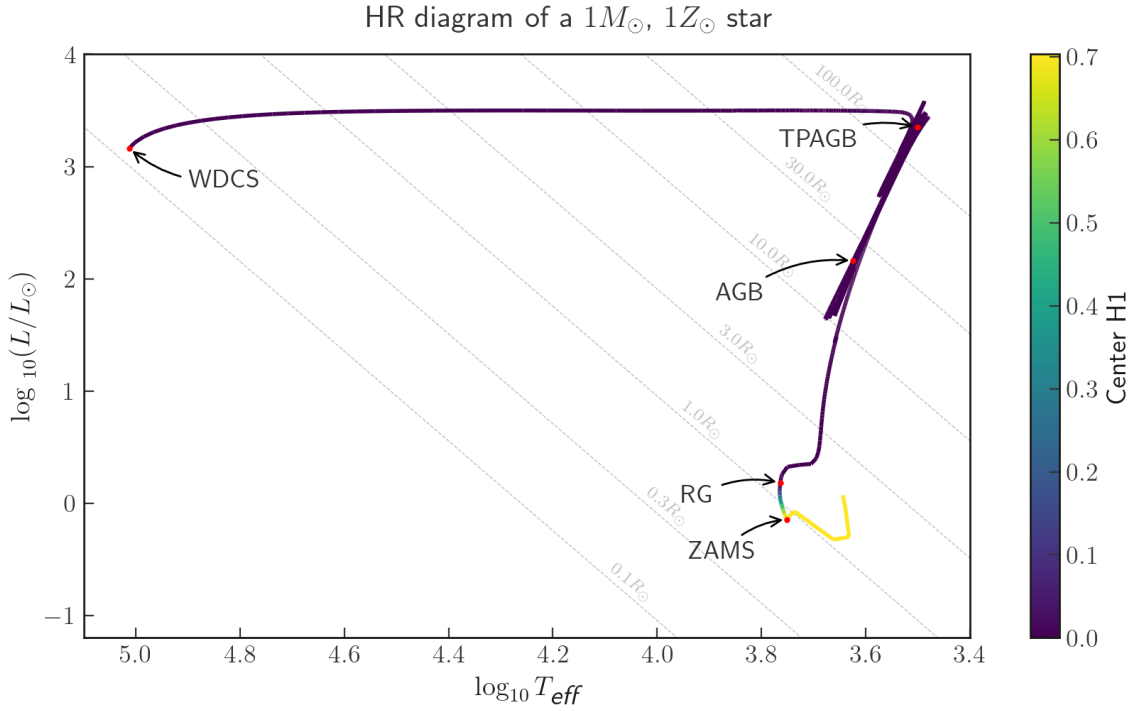


Figure 2.1: HR diagram track of a $1 M_{\odot}$, $1 Z_{\odot}$ star, before entering the main sequence (the starting point is labeled as ZAMS - Zero Age Main Sequence), on to the Red Giant branch (RG), the Asymptotic Giant Branch (AGB), Thermally Pulsating AGB (TPAGB) until it becomes a white dwarf and enters the White Dwarf Cooling Sequence (WDCS). The star track has been simulated with MESA.

2.1.2 Intermediate mass stars - convective cores

In stars with convective cores ($M_{\star} \gtrsim 1.3 M_{\odot}$) the material is well mixed, the core composition will evolve pretty homogeneously and the exhaustion of hydrogen will happen uniformly throughout the core.

Opacity decreases as hydrogen gets depleted, since the CNO cycle produces positrons that annihilate electrons: as a result, electron scattering is reduced. The consequence is that the extent of the convective core shrinks with time.

The outer layers of the star expand, and the effective temperature decreases, as it can be seen in the movement to the right of the stellar evolution track in the HR diagram.

The end of the main sequence is easily recognized in the HR diagram thanks to the

presence of a distinctive “left hook” (see figure 2.2 for $1.5 M_{\odot}$, $2 M_{\odot}$ and $3 M_{\odot}$). It corresponds to the final stage of hydrogen burning: when there’s little hydrogen, the core contracts, temperature and luminosity increase, and hydrogen is completely depleted in the core.

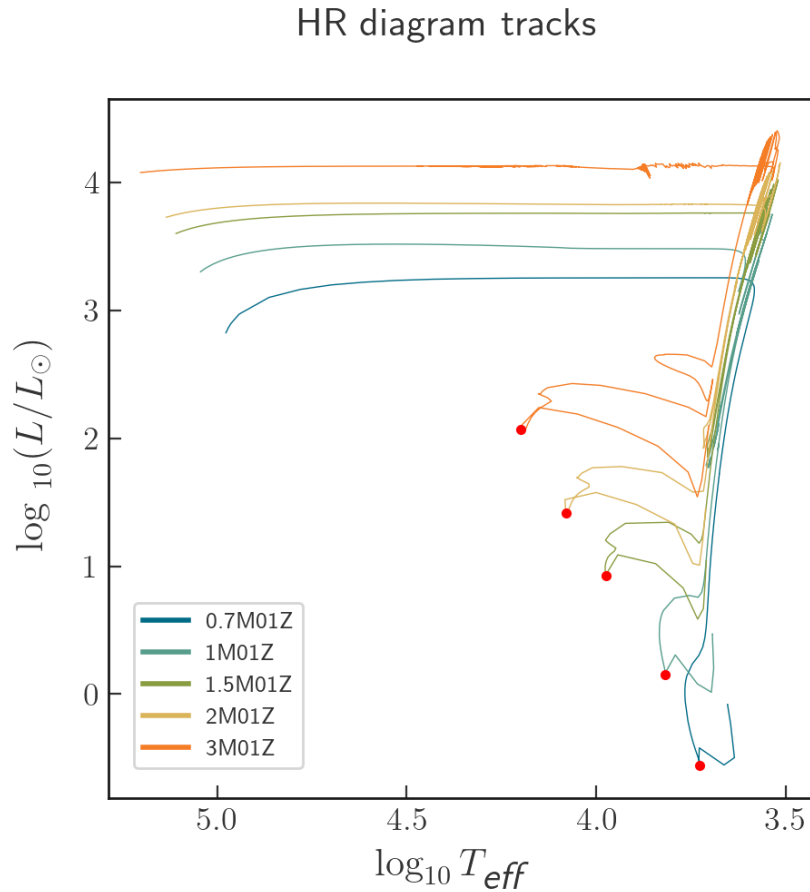


Figure 2.2: HR diagram tracks of $0.7 M_{\odot}$, $1 M_{\odot}$, $1.5 M_{\odot}$, $2 M_{\odot}$, $3 M_{\odot}$ stars with $0.1 Z_{\odot}$ metallicity, from the pre-main sequence until entering the white dwarf cooling sequence. The start of the main sequence is marked as a red dot. The star tracks have been simulated with the MESA stellar evolution code.

2.2 Red giant phase

2.2.1 Low mass stars

The star has a inhomogeneous structure at the core: inert helium at the center and a hydrogen shell around it. Helium fusion cannot take place at this stage, since the temperature is not high enough, so the core keeps contracting: half of the gravitational energy is released heating up the plasma, and the other half is radiated away, according to the virial theorem.

As the hydrogen shell contracts, the outer layers expand (see figure 2.4), obeying the mirror principle, and the effective temperature decreases. This is the red subgiant phase, which lasts $\sim 2 \times 10^9$ yr for solar-type stars: the star moves to the right in the HR diagram, up until the helium core becomes degenerate (from ZAMS to RG in figure 2.1), marking the start of the red giant phase, which will last $\sim 5 \times 10^8$ yr for a solar-type star.

At this point, the star climbs the HR diagram almost vertically because as the shell burns hydrogen, more helium gets deposited onto the helium core, which for a degenerate material means that the core contracts and heats up. The outer layers expand, cool and become fully convective (see the second panel of figure 2.5a). The mixing of the material in the center to the outer layers is referred to as “first dredge-up” (Herwig, 2005).

The star has developed a distinct internal structure, as illustrated in figure 2.3: the core is 10^6 times denser than the envelope, while during the main sequence, the core was denser only by a 10^2 factor. In section 3.3 we discuss why this is of extreme importance for tidal disruption events.

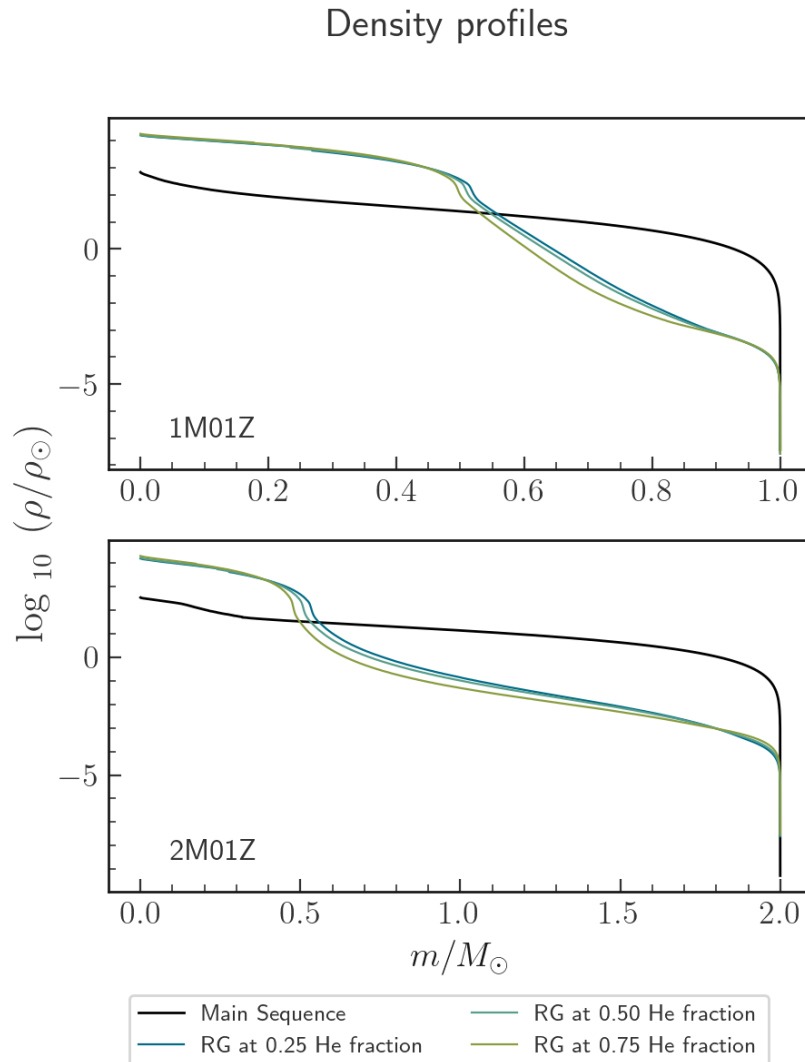


Figure 2.3: Density profile of $1 M_{\odot}$ and $2 M_{\odot}$ stars by the end of their main sequence (black lines) compared to different points in their red giant phase. During the red giant phase, the core is $\sim 10^6$ times denser than the envelope, while during the main sequence, the core is denser only by a 10^2 factor. The stars have been simulated with MESA.

The effective temperature remains approximately constant, but luminosity increases and the star becomes about 100 times bigger than in the main sequence phase.

The increasing size of the inert He core causes it to contract further, accelerating the hydrogen fusion rate. This is a runaway process that culminates in the explosive onset of Helium burning in the core: the temperature and density are finally high enough for the triple alpha process to start. This episode is called the Helium flash.

The strong shock waves remove the outer third of the star, so the stellar track moves to smaller radii, higher effective temperature and lower luminosity, in the horizontal branch. Solar metallicity stars will all lie in the same area of the HR diagram, called the “red clump”. The core is no longer degenerate and helium burning proceeds in a stable manner, for $\sim 1 \times 10^8$ yr for a solar-type star.

The star now has a He burning core surrounded by a H burning shell.

2.2.2 Intermediate mass stars

Stars with masses higher than $\sim 2 M_{\odot}$ are able to reach stable helium burning without the core becoming fully degenerate, so there is no helium flash.

The core shrinks and heats up, while the outer layers cool and expand (see figure 2.4), until helium fusion can begin in the center.

2.3 Asymptotic giant branch

The core has developed an inhomogeneous structure: an inert carbon and oxygen core surrounded by an inert shell of helium and a burning shell of hydrogen, as seen in the third panel of figure 2.5. The evolution is analogous to the red giant phase: the core contracts until it becomes degenerate and the outer layers expand according to the mirror principle. The star moves to higher radii, lower effective temperature and higher luminosities in an accelerated runaway process, approximately during $\sim 5 \times 10^6$ yr for solar-type stars.

The star goes through a second “dredge-up”, in which convection deepens until the core and the material in the center reaches the surface.

The increased temperature allows helium shell fusion to begin with a helium shell flash, triggering the expansion of the outer layers of the star.

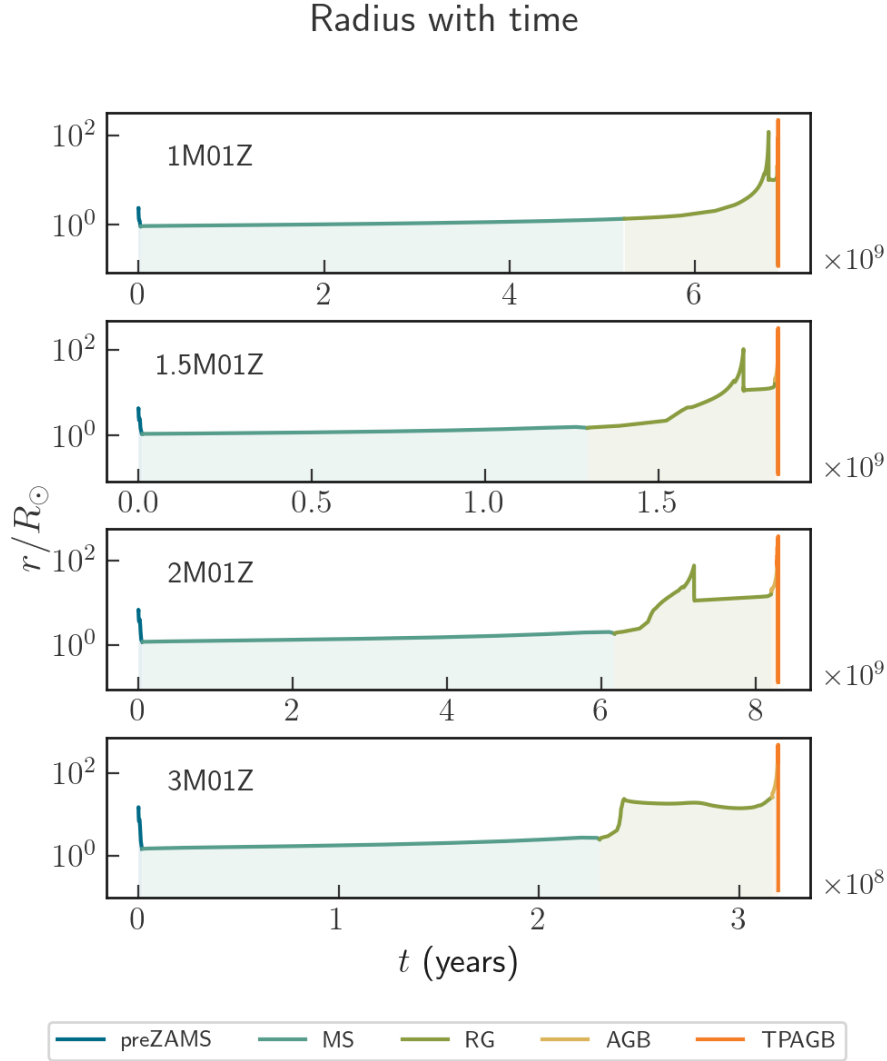


Figure 2.4: Radius as a function of time for the stars that we study, $1 M_{\odot}$, $1.5 M_{\odot}$, $2 M_{\odot}$ and $3 M_{\odot}$ with metallicity $0.1 Z_{\odot}$. Each stage of evolution is shaded in a different color. The stars have been simulated with the MESA stellar evolution code.

The star now enters the thermally pulsating AGB phase (TPAGB), in which the shells of hydrogen and helium fuse in alternate cycles or thermal pulsation. For stars with masses higher than $\sim 2 M_{\odot}$ there can be a third dredge-up (Herwig, 2005).

The duration of this phase is determined by the mass loss: at this stage there are strong winds that remove the H-rich envelope, which will be a planetary nebula (PN).

The star moves to the left in the HR diagram in the PN phase. Luminosity remains approximately constant, but the radius gets smaller and the effective temperature increases, until the star is left with a bare core.

Nuclear fusion is no longer possible. The degeneracy pressure balances out the gravity pull, and the star enters in the white dwarf cooling sequence (WDCS).

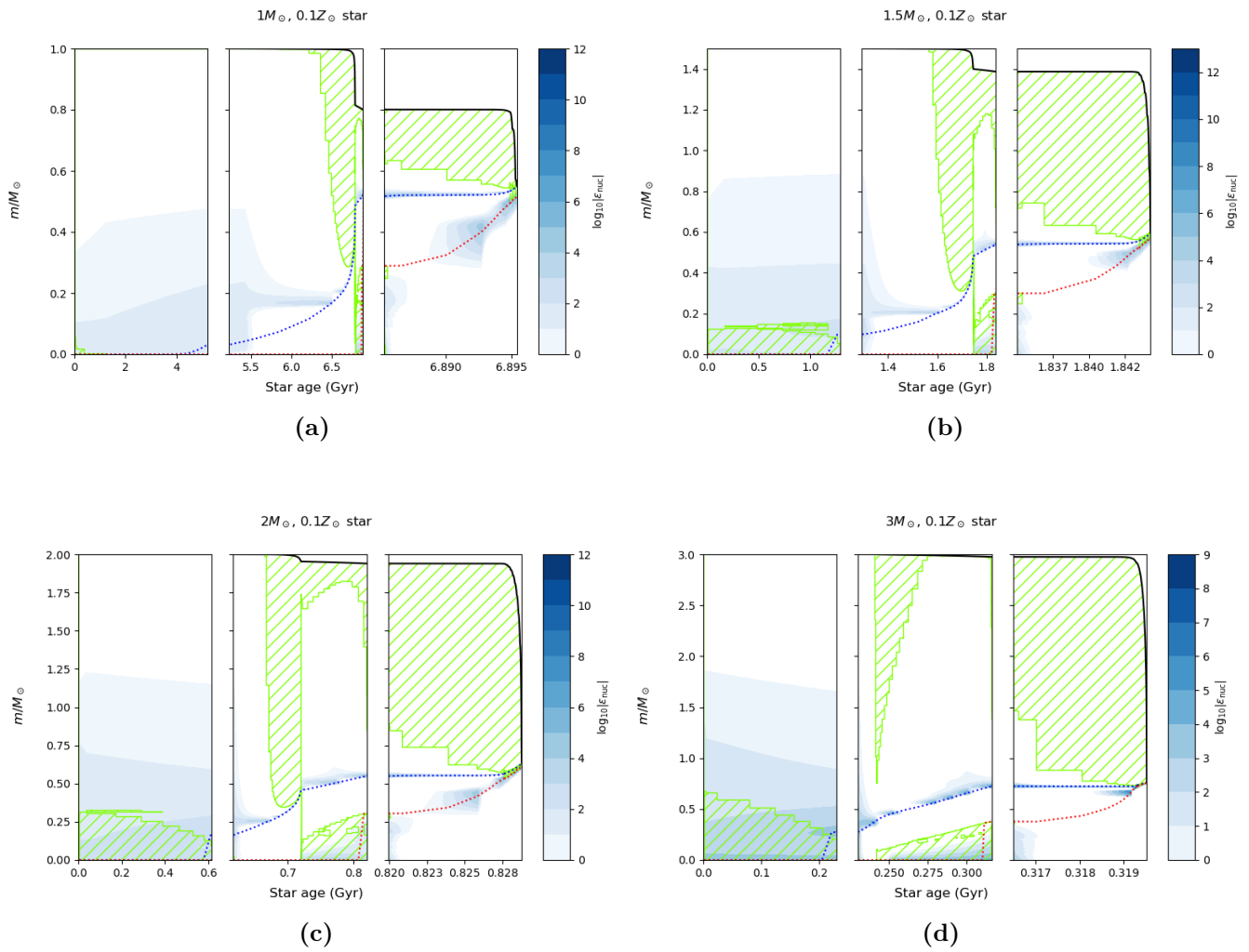


Figure 2.5: Kippenhahn diagrams of normal stars, in which the interior structure of the star is plotted with time. The first panel shows from the preZAMS to the terminal age Main Sequence (TAMS), the second panel shows the RG phase and the third panel shows from the start of the AGB to the WDCS. Hatched green areas correspond to convection zones, blue shading is nuclear energy, the blue dotted line shows the extent of the He core and the red dotted line shows the extent of the CO core.

3 Tidal disruption events

3.1 Tidal radius

If the tidal forces of a star are greater than its self-gravity, it will be torn apart, as [Hills \(1975\)](#) first observed. The approximate distance at which this happens is the tidal radius,

$$R_t \simeq R_\star \left(\frac{M_{\text{BH}}}{M_\star} \right)^{1/3} \quad (3.1)$$

where M_{BH} is the BH mass and M_\star , R_\star are the mass and radius of the star, respectively. In units of the gravitational radius of the black hole $r_g \equiv GM_{\text{BH}}/c^2$,

$$R_t \simeq 47 \left(\frac{M_{\text{BH}}}{10^6 M_\odot} \right)^{-2/3} \left(\frac{M_\star}{1 M_\odot} \right)^{-1/3} \left(\frac{R_\star}{1 R_\odot} \right) r_g \quad (3.2)$$

This is an estimation that doesn't account for the internal structure of the star or the relativistic effects, an accurate description of the "physical" tidal radius can be found in [Ryu et al. \(2020\)](#). For our purposes, the approximate tidal radius will suffice, since we will deal with cases in which $R_T \gg r_g$.

The expression can be raised to the third power and rewritten as follows,

$$\frac{M_\star}{R_\star^3} \simeq \frac{M_{\text{BH}}}{R_t^3}$$

Or in other words, the star’s density is approximately equal to an effective density,

$$\rho_\star \simeq \bar{\rho}_{\text{eff}} \quad (3.3)$$

Equation 3.3 is of special interest. The dynamical timescale of a star, also known as free-fall timescale, is

$$t_{\text{dyn}} \approx (G\rho_\star)^{-1/2} \quad (3.4)$$

On the other hand, assuming keplerian dynamics and parabolic orbits, the pericenter passage time is

$$t_p \approx \left(\frac{R_t^3}{GM_{\text{BH}}} \right)^{1/2} = (G\bar{\rho}_{\text{eff}})^{-1/2} \quad (3.5)$$

Therefore, from equation 3.3, the pericenter passage time is roughly equal to the dynamical timescale of the star,

$$t_p \approx t_{\text{dyn}} \quad (3.6)$$

3.2 Partial TDEs

Stars whose orbit approaches the tidal radius can suffer grazing encounters. The tidal forces are not strong enough to fully disrupt the star, but the outer layers of the envelope can be peeled off, a process we refer to as a partial tidal disruption event (PTDE). The resulting star is a “stripped” star, the object that will be the focus of our work.

The strength of the PTDE can be characterized by the penetration factor or impact parameter,

$$\beta = \frac{R_t}{r_p} \quad (3.7)$$

where r_p is the pericenter distance of the passing star. Thus, $\beta \gg 1$ is a deep encounter, $\beta \sim 1$ is a grazing encounter and $\beta_{\text{min}} < \beta < 1$ will be a PTDE, where β_{min} corresponds to the minimum penetration factor for a star to be partially disrupted (only loses the outmost part of the envelope) and depends on the internal structure

of the star.

3.3 PTDEs of Red Giants

As we have seen, red giants have a very distinct internal structure: a very dense core and a tenuous envelope. While for stars in the main sequence the ratio of core density to average density is of the order $\rho_c^{\text{MS}}/\bar{\rho}_*^{\text{MS}} \approx 10^2$, for red giants the ratio is four orders of magnitude greater $\rho_c^{\text{RG}}/\bar{\rho}_*^{\text{RG}} \approx 10^6$, as seen in figure 2.3. This is of critical importance in the context of TDEs. From equation 3.4 and 3.6,

$$t_{\text{dyn}}^c \ll t_{\text{dyn}}^{\text{env}} \approx t_p \quad (3.8)$$

that is, the dynamical timescale of the core is very small compared to the dynamical time of the envelope. Since the pericenter passage time is equivalent to the stellar dynamical time, the core won't be perturbed during the PTDE. Its gravitational influence will cause the envelope to rearrange itself as the encounter takes place, ultimately preventing the star from further mass loss (Hjellming & Webbink, 1987; Passy et al., 2012).

In figures 3.1 and 3.2 the tidal radius is plotted in gravitational radius units, $r_g = \frac{GM_{\text{BH}}}{c^2}$, against the stripped mass fraction $f_s = 1 - \frac{M(r)}{M_{\text{BH}}}$, from realistic red giant profiles calculated with the MESA stellar evolution code. The red-shaded area marks the interior of the black hole up until the the minimum pericenter r_p for parabolic orbits around a Schwarzschild black hole, at $r_p = 4r_g$, a value that is smaller for rotating black holes. Inside this region the star would simply plunge into the black hole.

For black holes with mass $M_{\text{BH}} = 10^6 M_{\odot}$ we see that stripping half of the mass of a $1 M_{\odot}$ star would require the star to reach the minimum pericenter distance, since the tidal radius at $f_s \approx 0.5$ is $R_t = 4r_g$. A bigger mass fraction can be stripped for stars with bigger masses, up to $f_s \approx 0.8$ for $3 M_{\odot}$, but for this case we never see

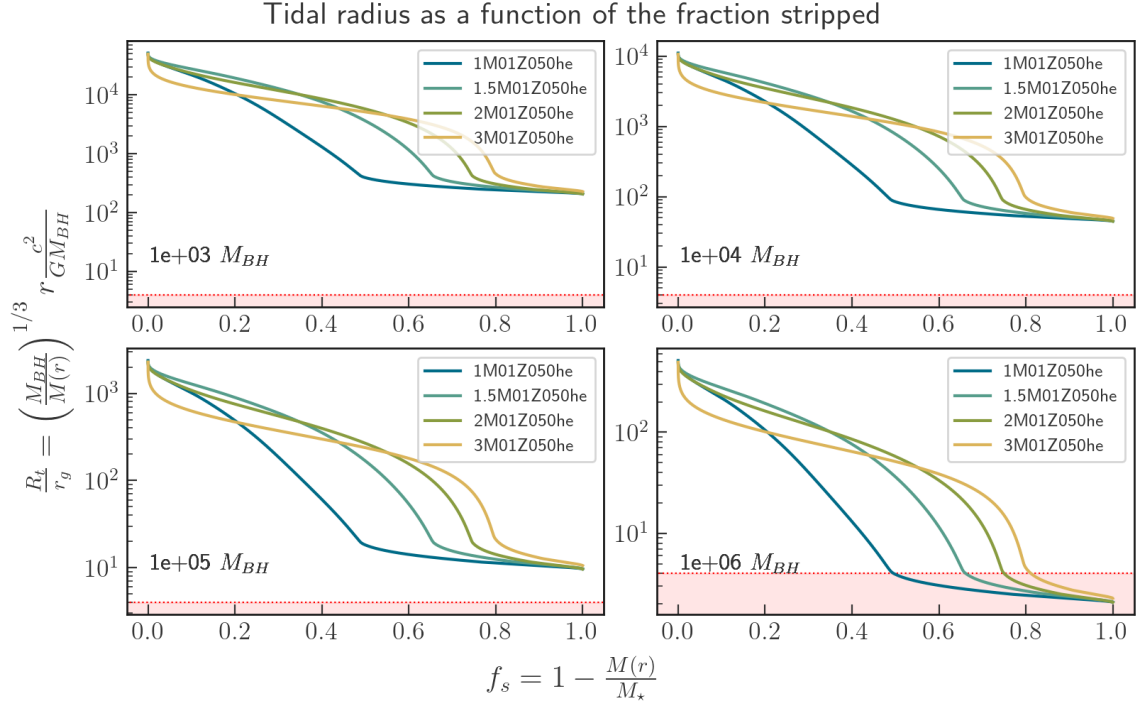


Figure 3.1: Tidal radius in units of gravitational radius as a function of the fraction of stripped mass, for MESA star models right before being stripped, when the Helium fraction is 0.50. The difference in the profile for each star is emphasized.

$f_s = 1$ out of the red region. Therefore, it is impossible to completely disrupt red giants for supermassive black holes, a result already shown by the hydrodynamic simulations carried out by MacLeod et al. (2012), implying that all giant-star TDEs for this kind of black holes are actually partial tidal disruptions (Rossi et al., 2021). However, as discussed in section 3.4, the likelihood of a tidal disruption is linearly proportional to the tidal radius. Therefore, partial tidal disruptions, especially of outer layers, are orders of magnitude more likely than full tidal disruption events. For example, disrupting only $f_s = 0.2$ of a $1 M_\odot$ star is about 45 times more likely than disrupting $f_s = 0.8$, for a black hole with mass $M_{BH} = 10^4 M_\odot$. The profile is flatter for higher stellar mass stars, but the result is the same: it is less likely to disrupt large mass fractions of a star than small mass fractions. Most TDEs of red giants will be partial disruptions of the outer layers of the star.

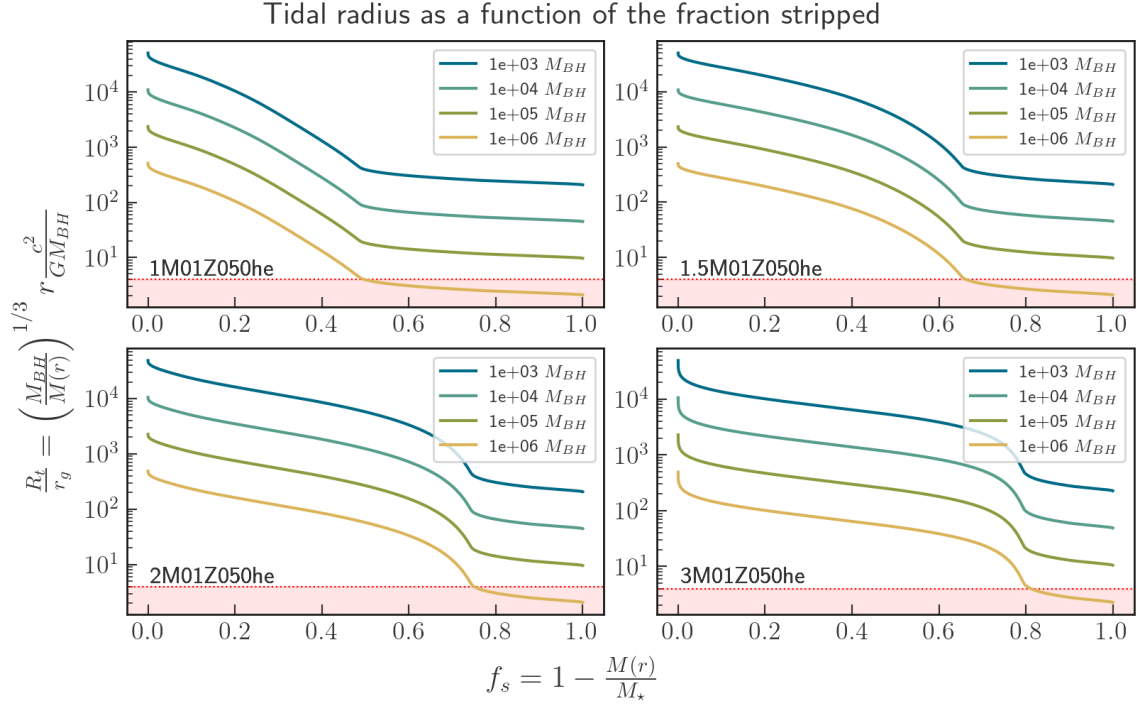


Figure 3.2: Tidal radius in units of gravitational radius as a function of the fraction of stripped mass, for MESA star models right before being stripped, when the Helium fraction is 0.50. The difference in the profile for each black hole is emphasized.

3.4 Rates

The specific orbital angular momentum of stars on nearly parabolic orbits, in Newtonian gravity, is $L \approx \sqrt{2GM_{\text{BH}}R_p}$. The stars with a lower orbital angular momentum than $L_{\text{crit}} \approx \sqrt{2GM_{\text{BH}}R_t}$ will reach the tidal sphere and as a result will be disrupted. The loss cone is the region in angular momentum space containing stars whose angular momentum is less than the critical value $L < L_{\text{crit}}$. Stars enter the loss cone through diffusion in the angular momentum, since it is faster than diffusion in energy (Frank & Rees, 1976). Because $L \propto R_t^{1/2}$, the total rate and thus the likelihood of TDEs is $\propto R_t$. The change in orbital angular momentum can be due to classical two-body scattering with other stellar objects or torques induced by an aspherical stellar potential (Stone et al., 2020).

The tricky part of estimating TDE rates lays in calculating the equilibrium loss

cone population. This involves knowing the distribution function of stars around the black hole and the details concerning the processes that change their angular momentum.

There are two limit regimes that are usually studied: the full loss cone or pinhole regime, when the typical change of angular momentum per orbital time is larger than the size of the loss cone, so stars are uniformly distributed inside and outside the loss cone, and the empty loss cone or diffusive regime, when the loss cone is scarcely repopulated. The total TDE rate can be calculated as contributions from both regimes.

An order of approximation can be found in [Rees \(1988\)](#):

$$\dot{N} \approx 10^{-4} M_6^{4/3} \left(\frac{N_\star}{10^5 \text{ pc}^{-3}} \right) \left(\frac{\sigma}{100 \text{ km/s}} \right)^{-1} \left(\frac{r_p}{R_t} \right) \text{ yr}^{-1}$$

where $M_6 = M_{\text{BH}}/10^6 M_\odot$, N_\star is the stellar density, σ is the velocity, r_p is the pericenter distance and R_t is the tidal radius.

There are two competing factors when talking about the TDE rates of red giant stars. Red giants have bigger radius than main sequence stars, which makes for larger tidal radius. As a result, the loss cone is bigger, which increases the rates approximately by a factor of $\sim R_{\text{RG}}/R_\star$ in the full loss cone regime and $\sim \ln(R_{\text{RG}}/R_\star)$ in the empty loss cone regime, which combined amount to a total of $\dot{N} \propto (R_{\text{RG}}/R_\star)^{1/4}$ ([MacLeod et al., 2012](#)). Furthermore, as first discussed in [Syer & Ulmer \(1999\)](#), red giants' radius is dependent on time and therefore stars can “grow into the loss cone”, further increasing the rate. However the lifetime of red giants is shorter than the lifetime of main sequence stars by a factor of 100, causing their population to be smaller and thus decreasing the rates.

Everything combined, the ratio between giant stars and main sequence stars TDE rates is approximately $\dot{N}_{\text{RG}}/\dot{N}_{\text{MS}} \sim 0.1$ ([Magorrian & Tremaine, 1999](#); [MacLeod et al., 2012](#)).

4 Methodology

4.1 MESA

We simulate the evolution of stripped red giants with the open source code Modules for Experiments in Stellar Astrophysics, (MESA, version r23.05.1; Paxton et al., 2011, 2013, 2015, 2018, 2019; Jermyn et al., 2023). MESA is a one-dimensional stellar evolution code, organized in independent, threadsafe modules that are called in the appropriate order by the module `star`. It is written in Fortran 90 and it is a Henyey style code (Henyey et al., 1959). Stars are sliced into cells, numbered from the surface to the core, for which the equations of stellar structure are solved separately. At each evolution step, a timestep is estimated, and the previous model of the star is adjusted. Re-meshing is performed if necessary, that is, some cells are split or merged according to the spatial resolution. Then, mass is adjusted to reflect mass loss by winds or mass gain from accretion, composition is adjusted, and the code proceeds to solve the equations of stellar structure for each slice of the star. It does so by using a variant of a Newton-Raphson solver, that is, iterating over trial solutions and adjusting parameters until numerical convergence is reached.

The different modules include the equation of state (`EOS`), opacities (`kap`), nuclear reaction networks (`net`) and others.

The MESA EOS is a blend of the OPAL (Rogers & Nayfonov, 2002), SCVH (Saumon et al., 1995), FreeEOS (Irwin, 2004), HELM (Timmes & Swesty, 2000), PC (Potekhin & Chabrier, 2010), and Skye (Jermyn et al., 2021) EOSes.

Radiative opacities are primarily from OPAL (Iglesias & Rogers, 1993, 1996), with low-temperature data from Ferguson et al. (2005) and the high-temperature, Compton-scattering dominated regime by Poutanen (2017). Electron conduction opacities are from Cassisi et al. (2007) and Blouin et al. (2020).

Nuclear reaction rates are from JINA REACLIB (Cyburt et al., 2010), NACRE (Angulo et al., 1999) and additional tabulated weak reaction rates Fuller et al. (1985); Oda et al. (1994); Langanke & Martínez-Pinedo (2000). Screening is included via the prescription of Chugunov et al. (2007). Thermal neutrino loss rates are from Itoh et al. (1996).

Convection is treated with the standard MLT of Cox & Giuli (1968). We use the Schwarzschild criterion for convective stability and the predictive mixing scheme, following Ostrowski et al. (2020) to avoid core splitting. We do not implement overshoot.

The Helium flash and thermally pulsing AGB (TPAGB) stages of evolution, if reached, are specially challenging. In order to reach numerical convergence, during those stages we use `eps_grav` as the `energy_eqn_option`, set to `true` `convergence_ignore_eqnL_residuals` and enable MLT++ with `okay_to_reduce_gradT_excess`.

We use Reimers (1975) for mass loss during the red giant phase, with a scaling factor $\eta_R = 0.477$ following McDonald & Zijlstra (2015). For the mass loss in the AGB phase we use Bloeker (1995) with a scaling factor $\eta_B = 0.1$.

4.2 Resolution tests

In order to explore numerical convergence we performed a series of resolution tests. We changed both spatial resolution with `mesh_delta_coeff` and temporal resolution with `time_delta_coeff` with values from 0.4 to 1.8 in steps of 0.2. Some of the final tests are plotted in figure 4.1. We chose to work with the parameters `mesh_delta_coeff = 0.6` and `time_delta_coeff = 1`.

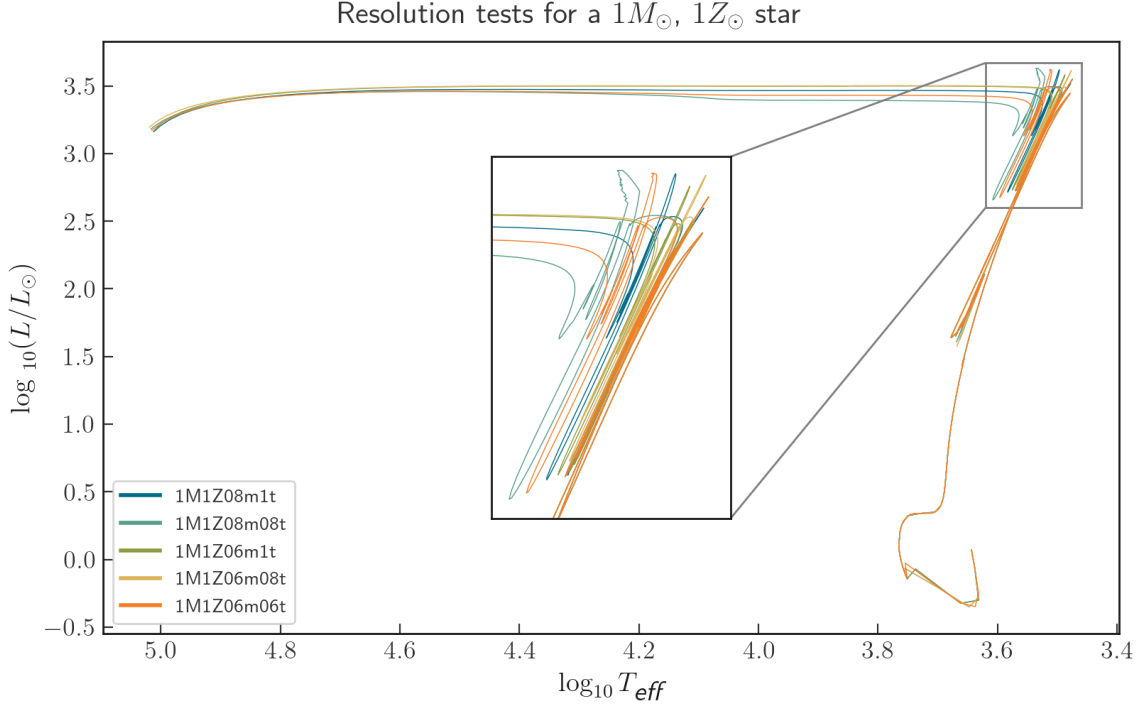


Figure 4.1: HR diagram track of a $1 M_{\odot}$, $1 Z_{\odot}$ star from preZAMS to WDCS for different values of temporal and spatial resolution, labeled in the legend by “m” (mesh) and “t” (temporal). The chosen final values correspond to the green line, “1M1Z06m1t”.

4.3 Simulating stripped stars

We evolve normal stars from the pre-main sequence up until different points in the red giant phase of evolution, using the Helium fraction as a stopping condition (at 0.25, 0.50 and 0.75). Then we proceed to peel off the outer layers.

The mass stripping in MESA is performed by gradually changing the total mass by a wind. The mass loss rate is estimated to be

$$\dot{M} \approx \frac{\Delta M}{t_p} \approx 1 M_{\odot}/\text{yr} \quad (4.1)$$

where t_p is the pericenter passage time (equation 3.5), of the order of 10^{-2} yr (calculated for the star masses explored with radii $\sim 10 - 30 R_{\odot}$, as discussed in section 5), and ΔM is the stripped mass, of the order of $10^{-1} M_{\odot}$.

The whole stripping process occurs through a MESA subroutine called `do_`

`internal_evolve`, in which the code evolves the star with the strong wind step by step until it reaches the desired new mass. Afterwards, the previous values for the star age and model are restored, so that the mass relaxation happens “internally”. This is a reasonable assumption, since the nuclear and thermal timescales are longer than the time the encounter lasts.

The whole process assumes hydrostatic equilibrium, a good assumption as discussed in section 3.3 when considering the mentioned timescales (equation 3.6). A further assumption is spherical approximation. Real partial tidal disruption events are highly aspherical: during the event the star’s stellar surface experiences quadrupole distortions and material from the envelope is ejected in two tidal tails. For red giants, the core is not distorted since the tidal force never overwhelms the self-gravity of the star, and we assume that the core’s gravity symmetrically rearranges the envelope.

All in all, the real process of stripping is more intricate and complicated. In order to confirm that all the assumptions are proper, we would need realistic PTDE simulations of red giants, which is a challenging endeavor because of the timescales for the core and the envelope. Simulations have been carried out by MacLeod et al. (2012), but instead of realistic red giants, polytropes were used.

The mass removal of the envelope is performed using the MESA flags `relax_initial_mass_to_remove_H_envelope` and `extra_mass_retained_by_remove_H_env`, equivalent to relaxing the mass to `new_mass = He_core_mass + extra_mass_retained_by_remove_H_env`. The mass loss rate is implemented in MESA through the flag `lg_max_abs_mdot = 0`.

The inlists used are published and can be downloaded in <https://doi.org/10.5281/zenodo.10156193>

5 Results

We have performed a total of 75 simulations. Taking $0.1 Z_{\odot}$ metallicity stars with a preZAMS mass of $1 M_{\odot}$, $1.5 M_{\odot}$, $2 M_{\odot}$ and $3 M_{\odot}$ we have stripped different mass quantities for each of them at helium fractions 0.25, 0.50 and 0.75 and evolved them until they reach the WDCS phase.

In figure 5.1 the different stripping times are plotted as red dots on a radius against time plot. We have chosen to strip at times in which the radius is representative of most of the red giant phase of the star. For example, even though a $1 M_{\odot}$, $0.1 Z_{\odot}$ star reaches a radius $R_{\star} \sim 80 R_{\odot}$ during the red giant phase, it constitutes only about $\sim 10^6$ years out of $\sim 1.5 \times 10^9$ years of its red giant phase. Our main goal is to study the general and representative cases, so we have left out of this work the special cases in which the stars reach large radii.

The density profiles of all stars at the moment of stripping are plotted in figures 5.2, 5.3 and 5.4. It can be seen that the inner structure is very similar: with the exception of the $3 M_{\odot}$ star, all the stars converge to a core that has the same extent in radius, mass, and density. The envelope shows variations in density and extent for each case.

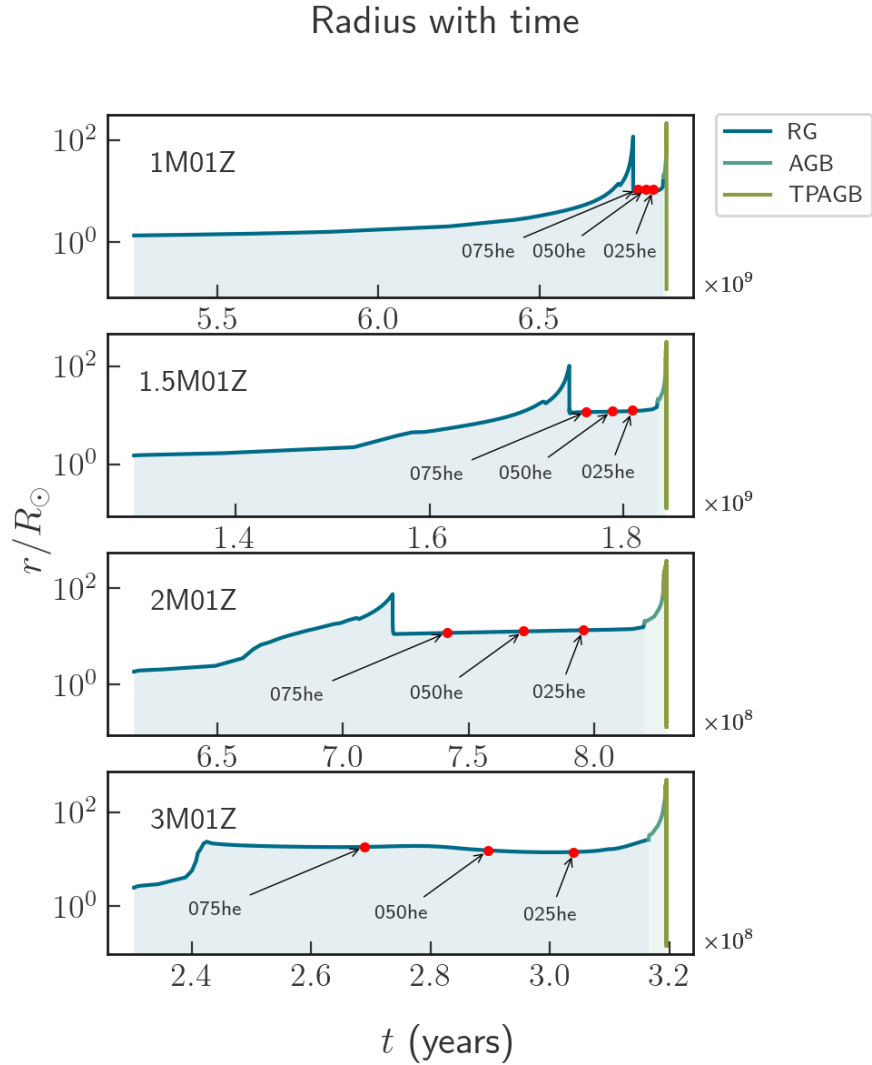


Figure 5.1: Radius as a function of time for the stars that we study, $1 M_{\odot}$, $1.5 M_{\odot}$, $2 M_{\odot}$ and $3 M_{\odot}$ with metallicity $0.1 Z_{\odot}$. The red dots indicate the three stripping times. The stars have been simulated with the MESA stellar evolution code.

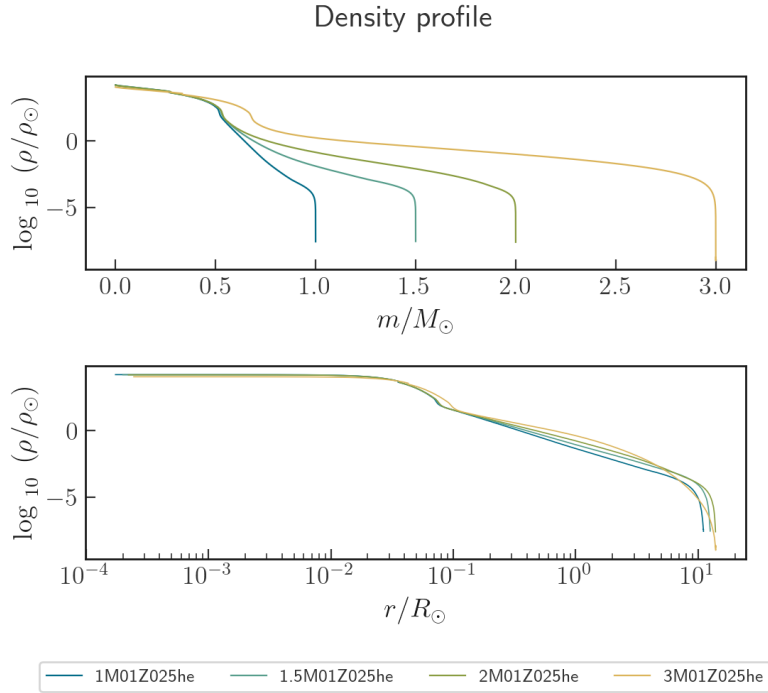


Figure 5.2: Density profile as a function of mass and radius for $1 M_{\odot}$, $1.5 M_{\odot}$, $2 M_{\odot}$ and $3 M_{\odot}$ stars at 0.25 helium fraction.

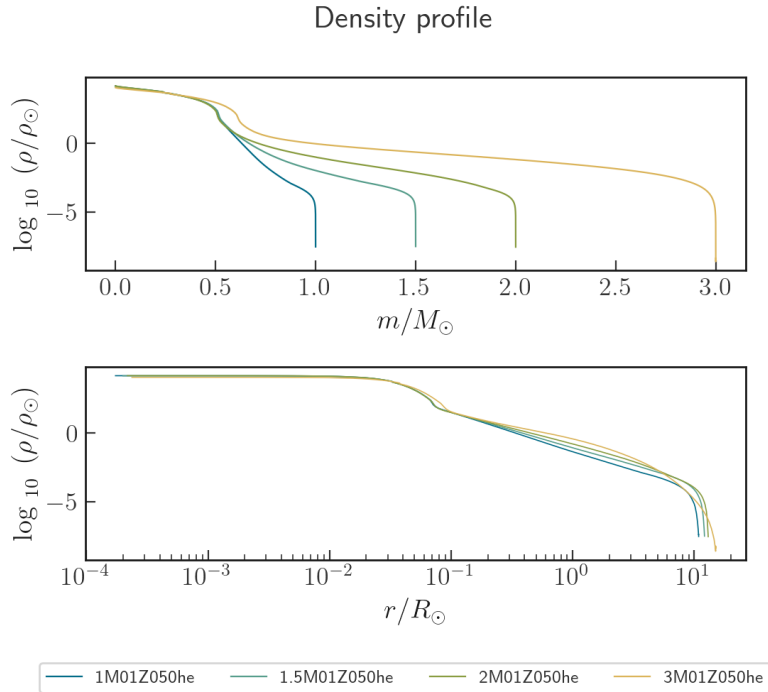


Figure 5.3: Density profile as a function of mass and radius for $1 M_{\odot}$, $1.5 M_{\odot}$, $2 M_{\odot}$ and $3 M_{\odot}$ stars at 0.50 helium fraction.

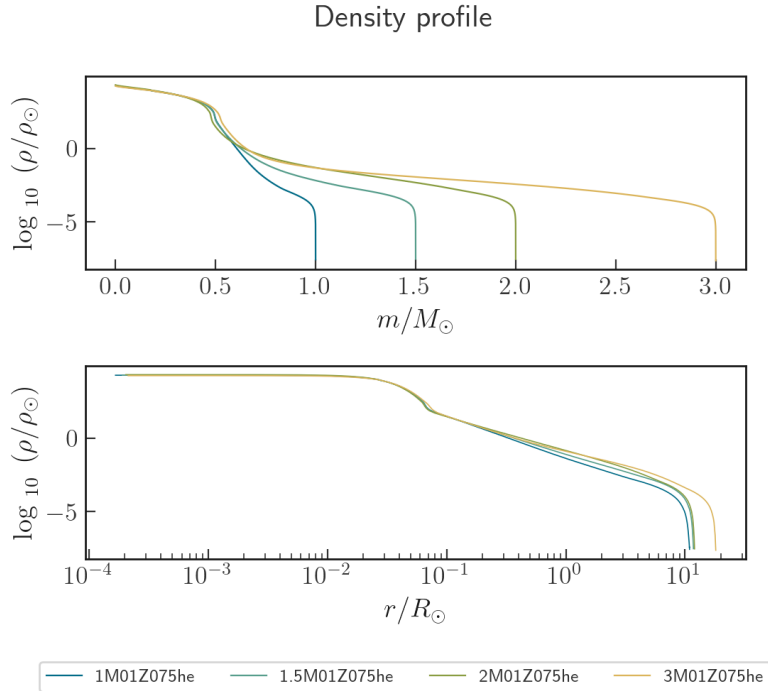


Figure 5.4: Density profile as a function of mass and radius for $1 M_{\odot}$, $1.5 M_{\odot}$, $2 M_{\odot}$ and $3 M_{\odot}$ stars at 0.75 helium fraction.

5.1 Star profiles before and after stripping

A first comparison can be done between the last model of the star before stripping and the first model of the star after stripping, as can be seen in figures 5.5, 5.6, 5.7, where the density and radius have been plotted against the mass. The blue line is always the star before stripping, the rest are the different stripped cases.

For a $1 M_{\odot}$ star, the stripping time is not relevant, figures 5.5a 5.5b and 5.5c show the same behaviour. The only difference is the total mass of the resulting stripped stars. Looking at the stripped case labeled 082m052c, we see that the envelope becomes more tenuous as described in section 3.3, since the outer layers of the star have expanded. On the other hand, the most stripped case, labeled 062m052c—which is also the less likely case, as we have previously discussed—doesn't recover the red giant internal structure, the mass retained is too little, and the expansion

of the outer layers is minimal.

For $1.5 M_{\odot}$ and $2 M_{\odot}$ stars (figures 5.6 and 5.7) we see the same behavior. The more mass is taken in the stripping process, the less expands the resulting star. The density profiles indicate that the stripped stars recover the red giant structure.

On the other hand, the $3 M_{\odot}$ star stripped at 0.25 and 0.50 helium fraction (figures 5.8a and 5.8b) show a different behaviour: the stripped stars expand very little immediately after the stripping, in contrast to the earliest stripped case shown in figure 5.8c, possibly due to a combination of the remaining helium available for burning and the core mass.

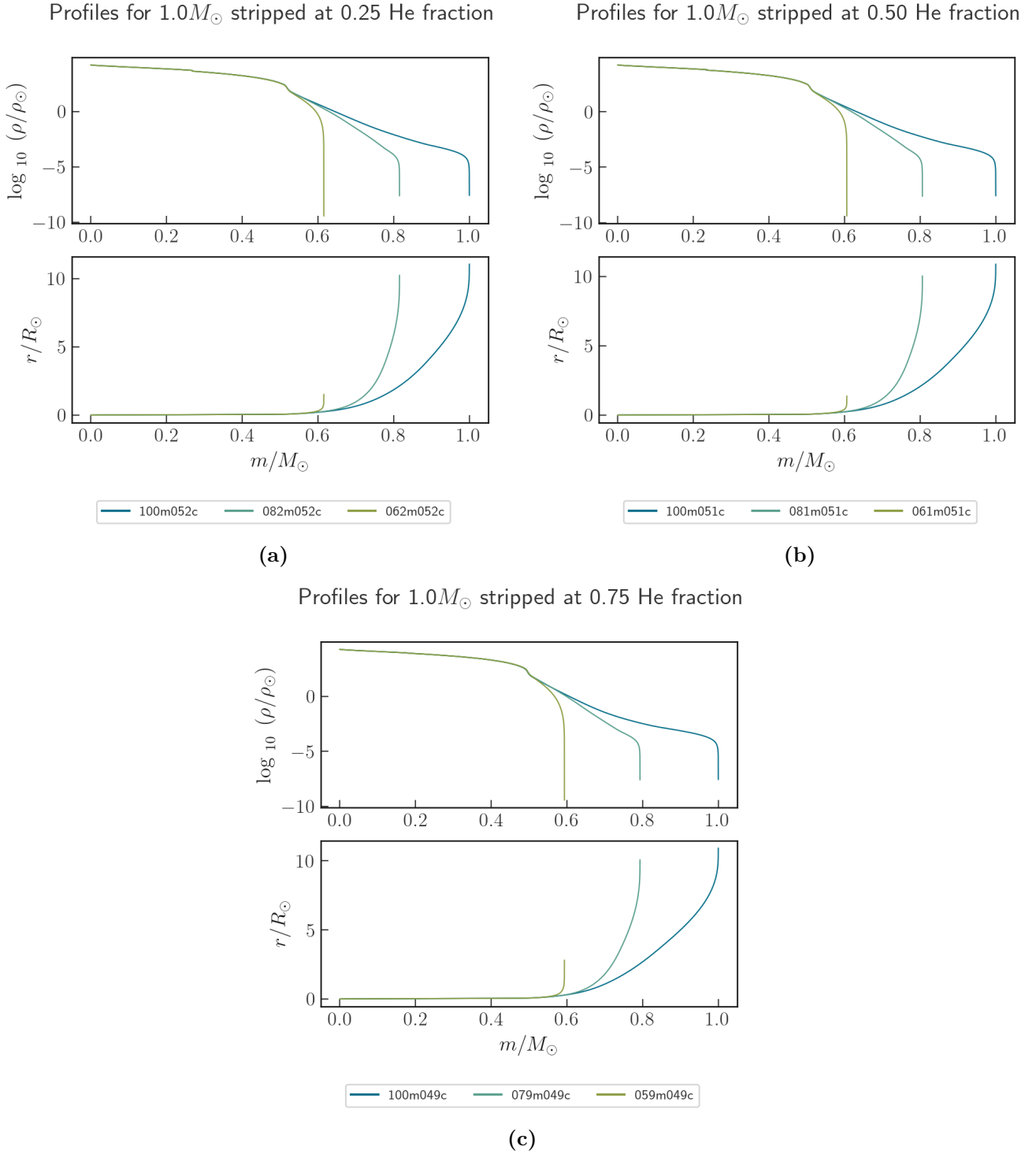


Figure 5.5: Density and radius against the m lagrangian coordinate before (blue line) and after stripping a $1 M_{\odot}$ star, for different stripping times, characterized by the helium fraction. The number before “m” indicates the total resulting mass (100 is 1.00) and the number before “c” indicates the core mass.

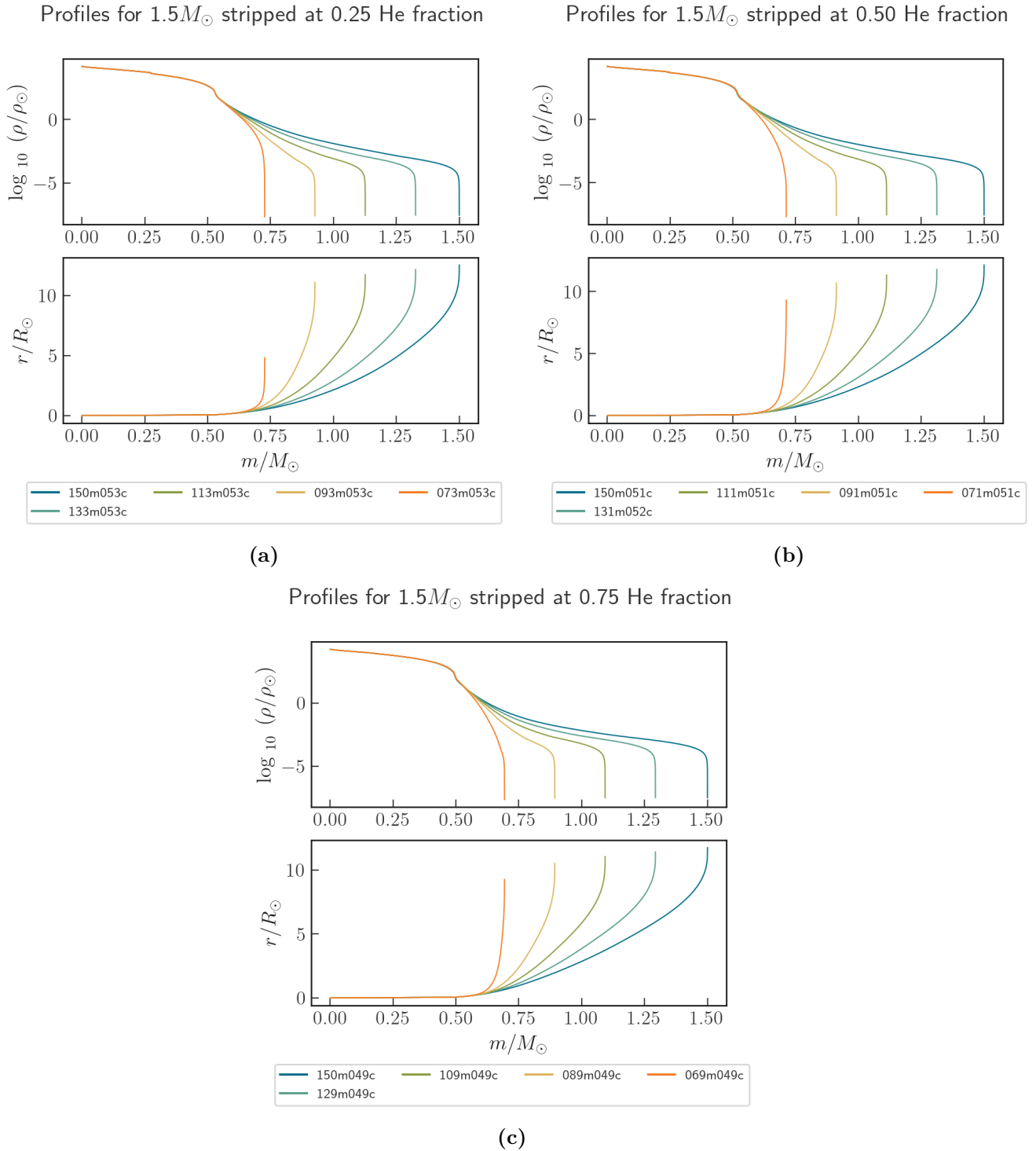
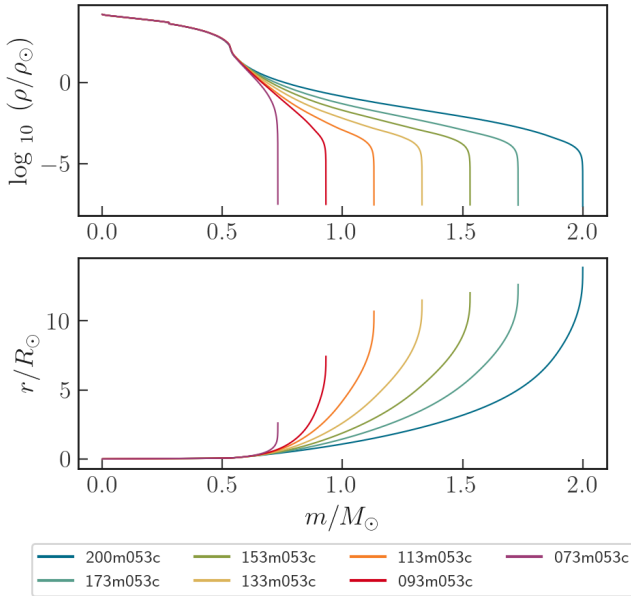


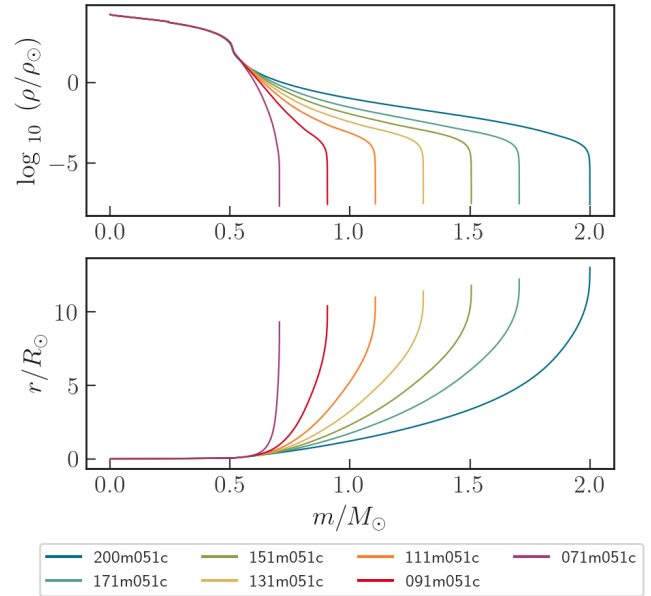
Figure 5.6: Density and radius against the m lagrangian coordinate before (blue line) and after stripping a $1.5 M_{\odot}$ star, for different stripping times, characterized by the helium fraction. The number before “m” indicates the total resulting mass (150 is 1.50) and the number before “c” indicates the core mass.

Profiles for $2.0M_{\odot}$ stripped at 0.25 He fraction



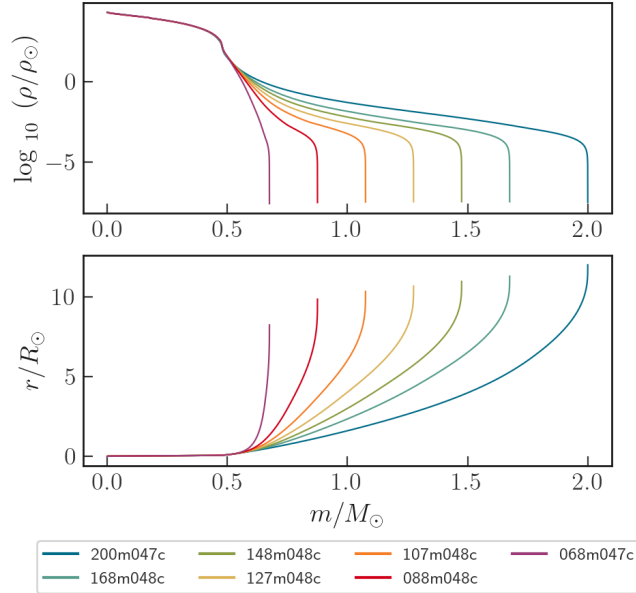
(a)

Profiles for $2.0M_{\odot}$ stripped at 0.50 He fraction



(b)

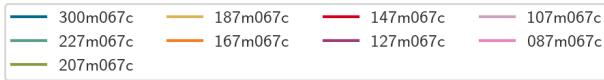
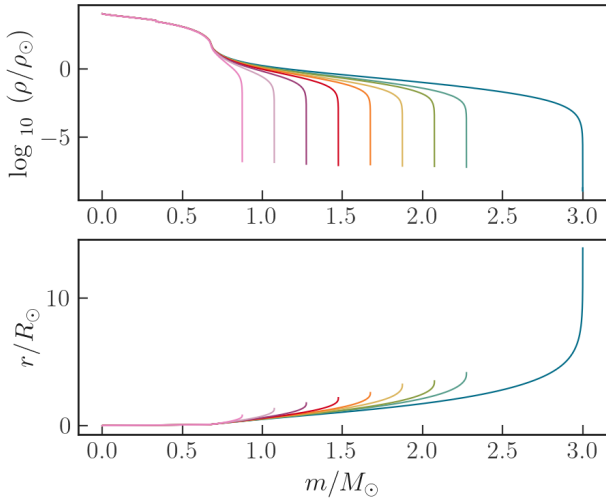
Profiles for $2.0M_{\odot}$ stripped at 0.75 He fraction



(c)

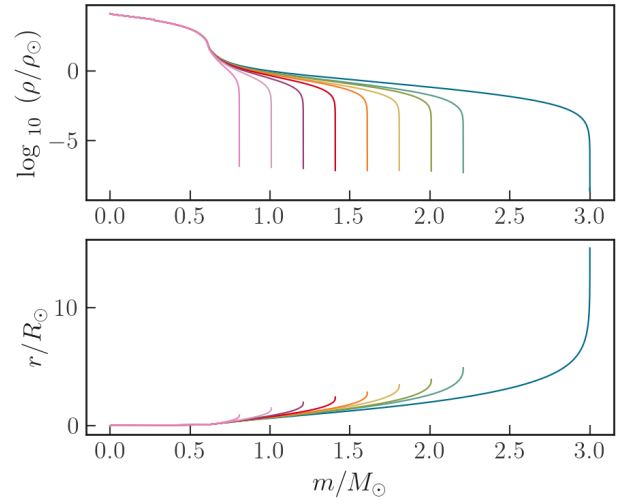
Figure 5.7: Density and radius against the m lagrangian coordinate before (blue line) and after stripping a $2 M_{\odot}$ star, for different stripping times, characterized by the helium fraction. The number before “m” indicates the total resulting mass (200 is 2.00) and the number before “c” indicates the core mass.

Profiles for $3.0M_{\odot}$ stripped at 0.25 He fraction



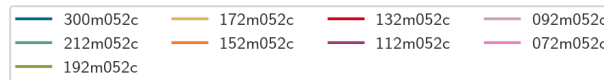
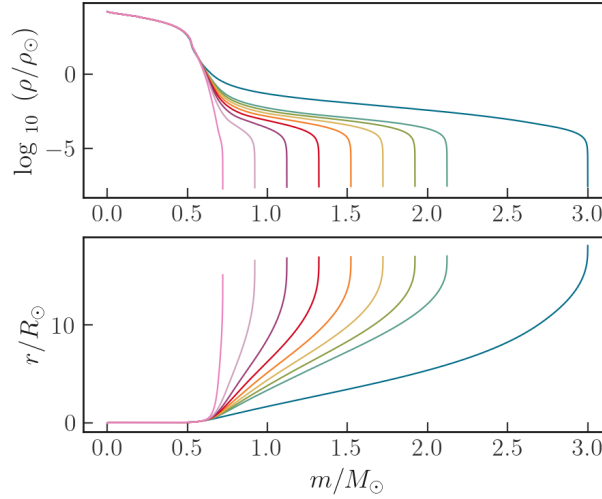
(a)

Profiles for $3.0M_{\odot}$ stripped at 0.50 He fraction



(b)

Profiles for $3.0M_{\odot}$ stripped at 0.75 He fraction



(c)

Figure 5.8: Density and radius against the m lagrangian coordinate before (blue line) and after stripping a $3 M_{\odot}$ star, for different stripping times, characterized by the helium fraction. The number before “m” indicates the total resulting mass (300 is 3.00) and the number before “c” indicates the core mass.

5.2 Long-term evolution

Stars whose envelope has been completely stripped die automatically, that is, the bare core becomes a helium white dwarf in a brief period of time. We have already discussed that this case is very unlikely (see section 3.3). Stars that partially retain their envelope, however, continue their life in the red giant phase. As seen for four different stripped stars in figure 5.10, stripped stars do not drastically change their internal structure: after the stripping, the core remains convective and burning, in some cases (figures 5.10a, 5.10b) the nuclear energy burning rate decreases.

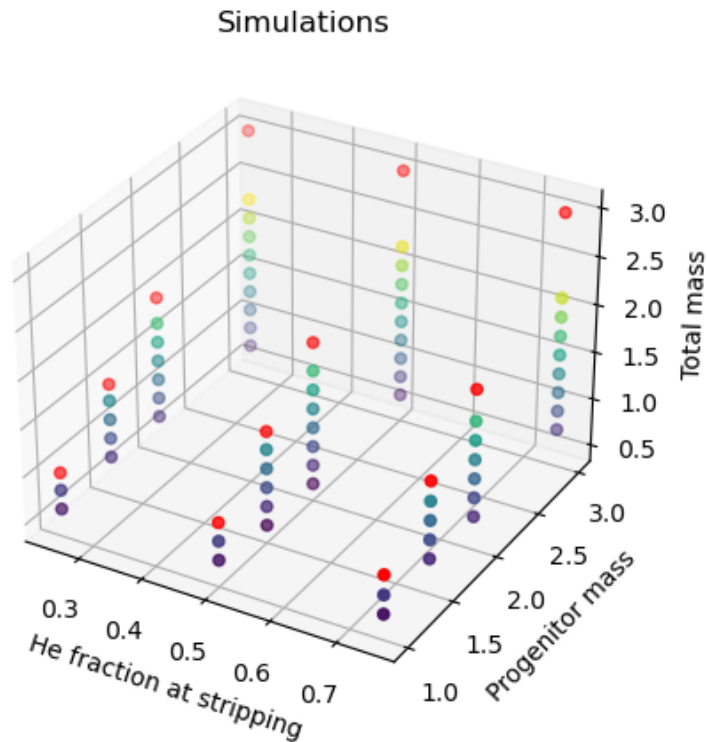


Figure 5.9: Each dot corresponds to a MESA simulation. Red dots are normal stars, the rest are stars that have been stripped, separated on intervals of $0.2 M_{\odot}$.

The three relevant parameters explored in our results are: the total mass of the resulting star (after the stripping), the progenitor mass (the preZAMS mass of the model) and the stripping time (characterized by the helium fraction). All the sim-

ulations are represented in the parameter space in figure 5.9.

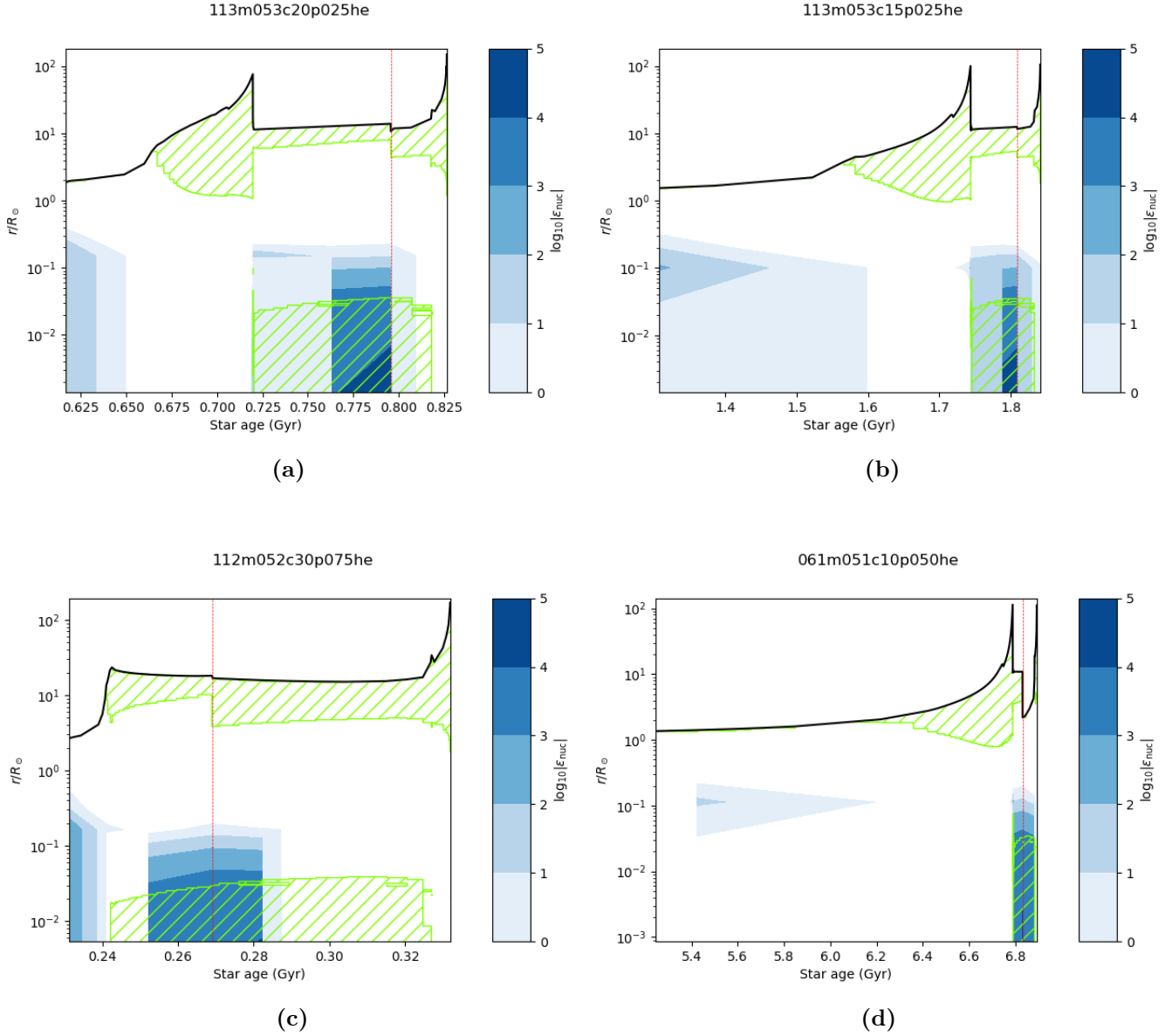


Figure 5.10: Kippenhahn diagrams of stripped stars. The plot starts in the beginning of the RG phase and finishes when the star enters the WD phase. The time of the stripping is marked with a dashed red line. Hatched green areas correspond to convection, and the blue shading is nuclear energy. The labeling goes as follows: $\#.\#\#m$ is the total resulting mass, $\#.\#\#c$ is the core mass, $\#.\#\#p$ is the progenitor mass and $\#.\#\#he$ is the helium fraction at the stripping time. All mass quantities have M_\odot units.

We have compared the results of the simulations in the three different axes as follows.

5.2.1 Progenitor mass comparison

Progenitor star and stripped stars comparison

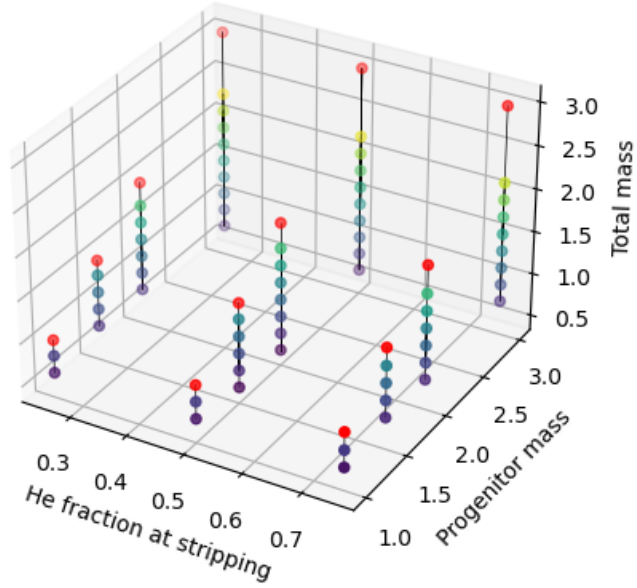


Figure 5.11: Each dot corresponds to a MESA simulation. Red dots are normal stars, the rest are stars that have been stripped, separated on intervals or $0.2 M_{\odot}$. The lines connect the results that have been compared.

Stripped stars compared with their progenitor star present a series of common features. With the exception of the totally stripped case (bare core), the stripped stars' envelope expands after the stripping until the radius is approximately that of the progenitor star before the stripping, as already seen in section 5.1. The envelope becomes more tenuous, as a result, which could make them vulnerable to a second stripping.

Stars that are totally stripped of their envelope quickly enter the white dwarf cooling sequence right after being stripped.

The luminosity of stripped stars is lower than the luminosity of their progenitor star, as can be seen in figure B.1 in the Appendix.

Some of the tracks in figures B.1, B.2 and B.3 show loops in the planetary nebula (PN) phase. This is called a late thermal pulse, it consists on a helium shell flash after the AGB phase that causes a rapid looping evolution between the AGB and PN phase. It should be regarded as an artifact of the parameters of the simulation and not as a characteristic feature of the stripped star, since the results at these stages are very sensitive to input physics.

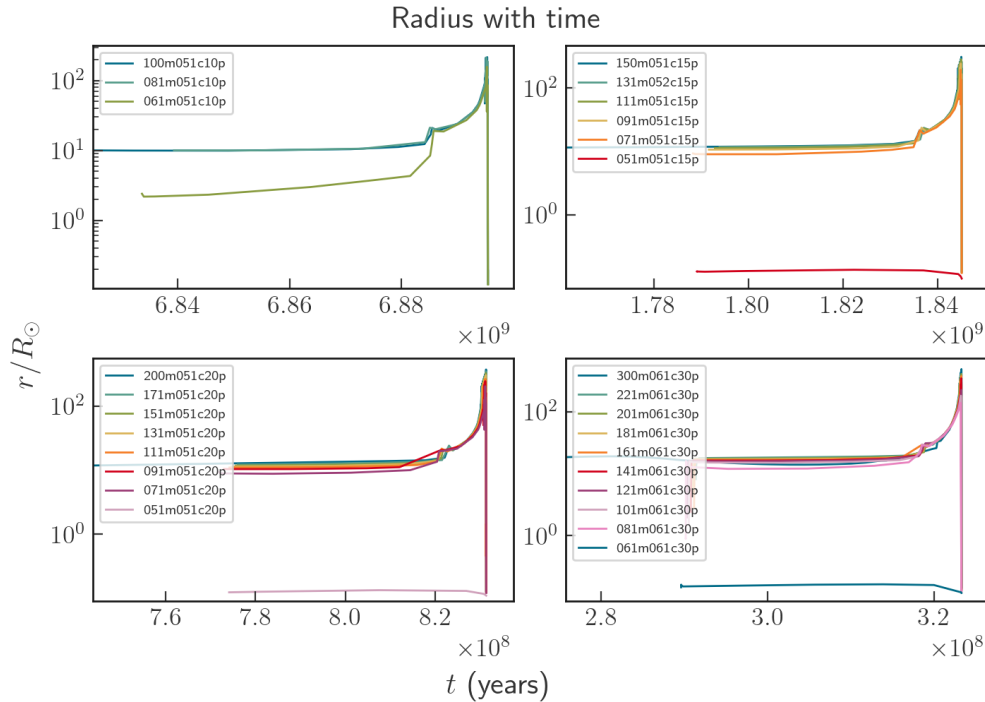


Figure 5.12: Radius with time of stars stripped at 0.50 helium fraction compared to their progenitor. The time coordinate has been shifted so that they all become white dwarfs at the same time.

In figure 5.12 the behaviour of the radius during the last stages of the stars is plotted. The time coordinate has been shifted so that the stars become white dwarfs at the same time. This allows us to see that the radius of the stripped stars is very similar to the progenitor's radius during the late stages of their evolution, with the exception of the fully stripped cases.

All stars stripped at later stages (0.25 helium fraction) die earlier than their progenitor stars, since there is less helium left to burn. However, stars stripped earlier

(at 0.75 helium fraction) die later than their progenitor star. They still have plenty of helium to burn but their total mass has been reduced, so they behave like low-mass red giants and have longer lifetimes. The transition between both situations is found when stripping at 0.50 helium fraction: some stripped cases live longer than the progenitor stars and some stripped cases have their lives shortened. For example, a $1.5 M_{\odot}$ normal star dies approximately at the same time as the stripped cases (from a $1.5 M_{\odot}$ star progenitor) with total mass $M_{\star} = 0.9 M_{\odot}$ and $M_{\star} = 1.1 M_{\odot}$. The stripped star with total mass $M_{\star} = 0.7 M_{\odot}$ dies later, and the stripped star with total mass $M_{\star} = 1.3 M_{\odot}$ dies earlier.

All the differences in the lifetimes of stripped stars when compared to their progenitor star, be it an earlier death or a prolonged life, are of the order of $\sim 1 - 5 \times 10^6$ years. Compared to the duration of the red giant phase ($\sim 10^8$ for $0.1 Z_{\odot}$ stars with intermediate mass, $\sim 10^9$ for the $1 M_{\odot}$ star), it constitutes a brief period of time, especially for lower mass stars.

5.2.2 Total mass comparison

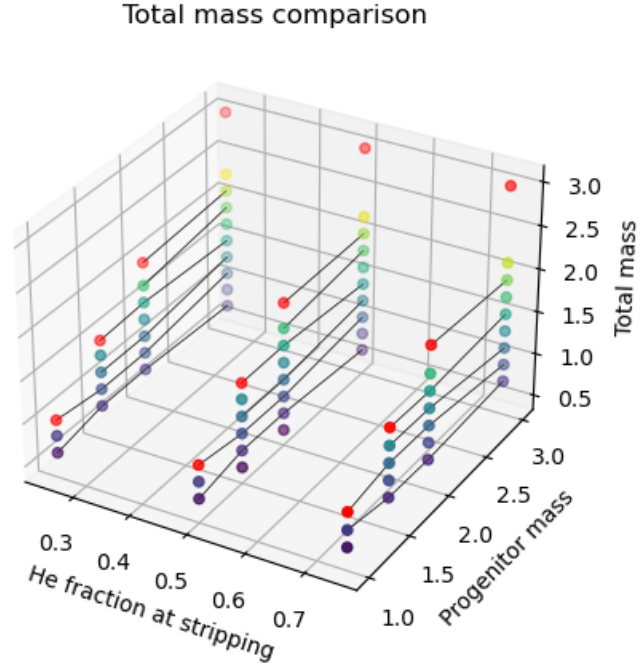


Figure 5.13: Each dot corresponds to a MESA simulation. Red dots are normal stars, the rest are stars that have been stripped, separated on intervals of $0.2 M_{\odot}$. The lines connect the results that have been compared.

Next, we have compared stars with the same total mass ($\Delta M_{\star} = \pm 0.095 M_{\odot}$). In the HR diagram (see figure B.2) stars behave very similarly, again, with the exception of the fully stripped cases, which enter the WDCS right after being stripped.

In figure 5.14 we show the stellar tracks of stars with total mass $M_{\star} = (0.7 \pm 0.05) M_{\odot}$ after stripping, compared to the track of a normal preZAMS $0.7 M_{\odot}$ star (black thick line). The luminosity of the stripped stars is higher, because their core is always more massive. The normal preZAMS $0.7 M_{\odot}$ star by the end of its red giant phase has a core $M_c \simeq 0.46 M_{\odot}$ and has lost all of its envelope.

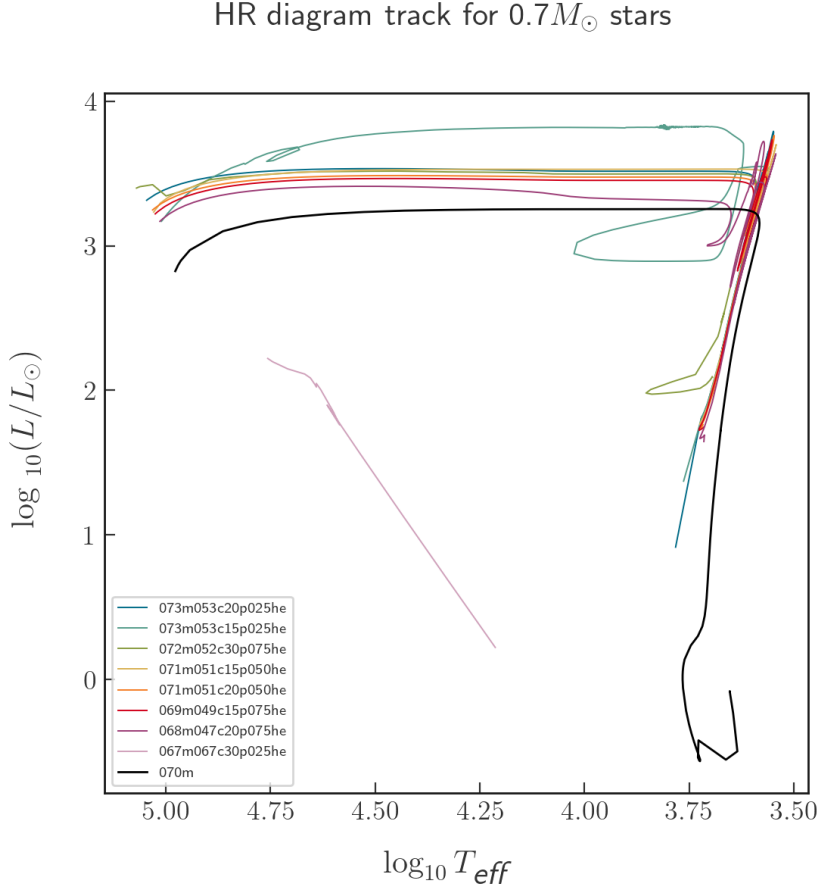


Figure 5.14: HR diagram tracks for stars of $0.7 \pm 0.05 M_{\odot}$ mass at stripping time and a normal preZAMS $7 M_{\odot}$ star (black, thick line). The stellar tracks have been simulated with the MESA stellar evolution code. Labels have the following structure, with the quantities measured at the time of stripping: #.##m indicates the total mass, #.##c is the core mass, #.##p is the progenitor mass, and #.##he is the helium fraction. All masses are expressed in units of M_{\odot} .

It is important to remark that a normal $0.7 M_{\odot}$, $0.1 Z_{\odot}$ star enters the red giant phase at $t = 2.16 \times 10^{10}$ yr, a time larger than the age of the universe. From this, we can conclude that observed red giants with low masses necessarily come from partially stripped stars. The uncertainty lies in whether these stars were stripped during a PTDE, due to strong winds, or binary mass transfer, as is the case in Li et al. (2022), followed by the loss of its companion.

In figure 5.15 the radius with time (shifted so that they all become white dwarfs at the same time) is plotted for four different cases of stripped stars and normal

stars with the same total mass. Again, the radii are all similar, regardless of the progenitor star. The latest stages show thermal pulsations for all stars exceeding $1 M_{\odot}$. The number of pulsations depends on the input physics, as explained in chapter 4, so it should not be regarded as an important feature of the figure.

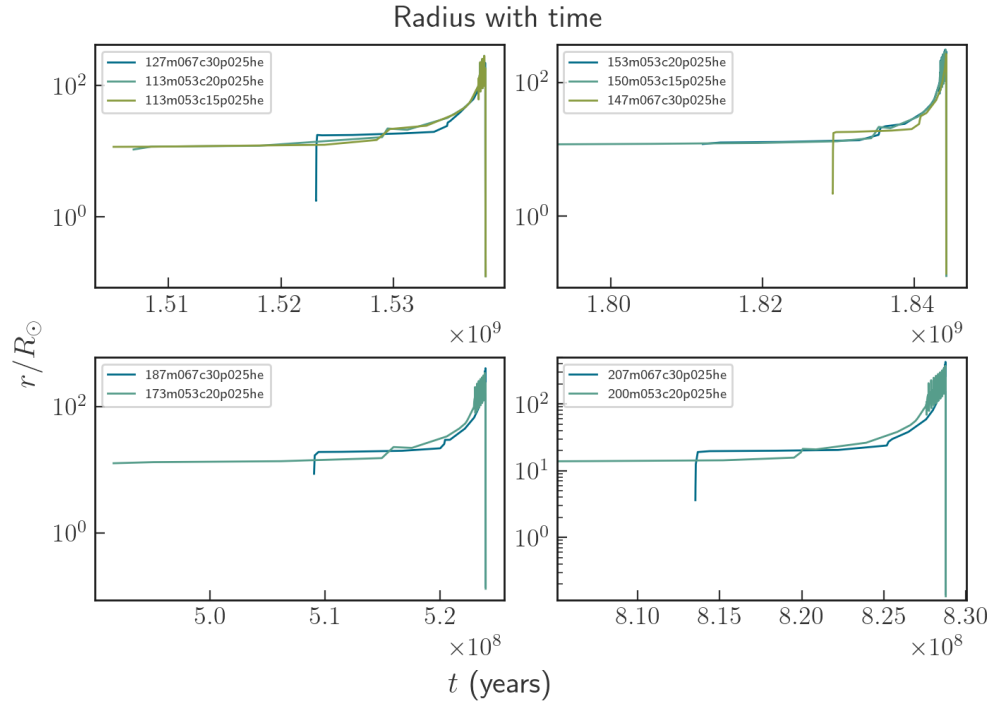


Figure 5.15: Radius with time of stars with the same total mass. The time coordinate has been shifted so that they all become white dwarfs at the same time.

Figures 5.2, 5.3 and 5.4 explain the similar behaviour for all stripped stars with the same total mass. The core shows essentially the same features, and therefore, the resulting stripped stars will be very similar.

5.2.3 Stripping time comparison

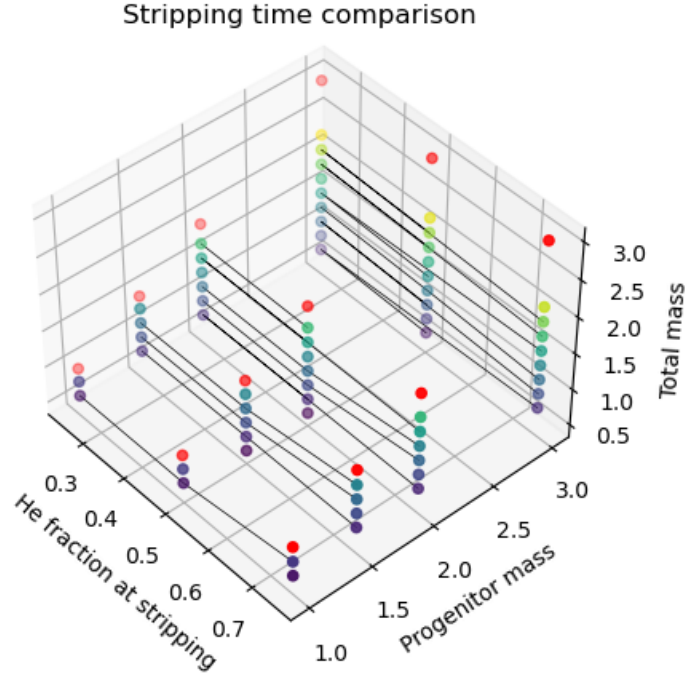


Figure 5.16: Each dot corresponds to a MESA simulation. Red dots are normal stars, the rest are stars that have been stripped, separated on intervals of $0.2 M_{\odot}$. The lines connect the results that have been compared.

Stars with the same total mass ($\Delta M_{\star} = \pm 0.098 M_{\odot}$), the same progenitor mass and different stripping times have been compared. As shown in figure B.3, the HR diagram tracks are very similar. The subtle difference in luminosity comes from the mass: more massive stars will be slightly more luminous, as one would expect. Therefore, we can conclude that the difference in the helium fraction at the stripping time is negligible.

The evolution of the radius with time is plotted for some stars in figure 5.17, with the time coordinate shifted so that all stars become white dwarfs at the same time. The stripped stars, no matter when they were stripped, behave similarly. The only difference is in their lifetime.

Stars that were stripped later are the first to die —a reasonable result, since their helium fraction is lower.

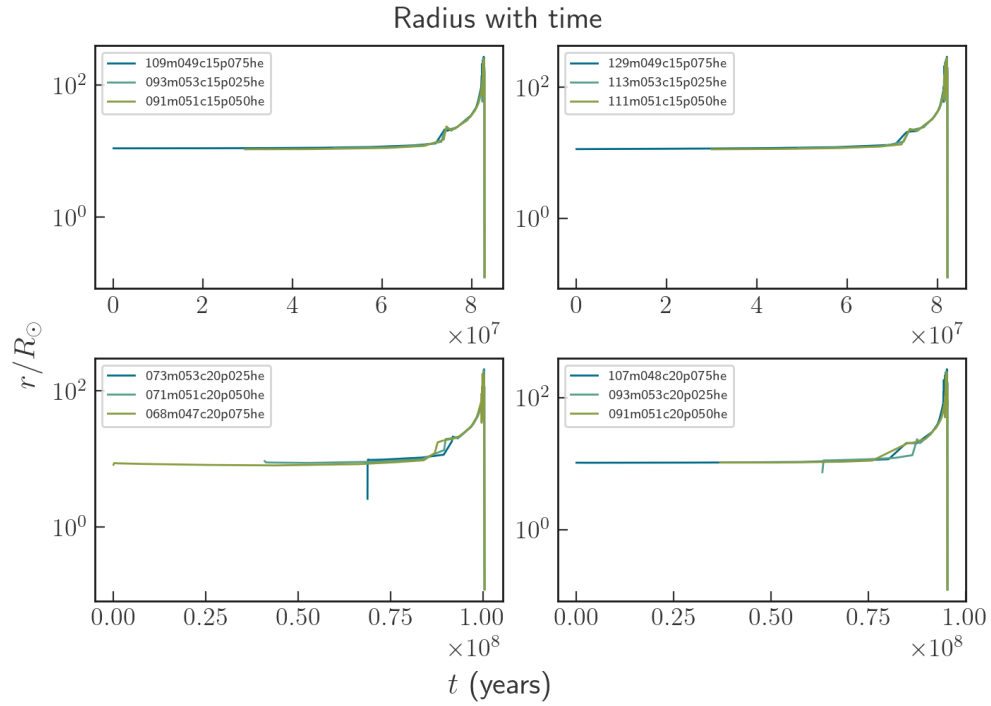


Figure 5.17: Radius with time of stars stripped at different times. The time coordinate has been shifted so that they all become white dwarfs at the same time.

6 Conclusion

We highlight the importance of partial tidal disruption events of red giants within the broader category of tidal disruption events, and in particular, we remark the most probable scenario involves the stripping of only a small fraction of the red giant's envelope mass. We strip realistic red giant stars with the MESA stellar evolution code, treating the stripping as carried out by an artificial wind, assuming spherical symmetry and neglecting the evolution of the star during the stripping process. The simulation of the long-term evolution of the remaining stars is a challenging one, since the late RG, the AGB and TPAGB phases are complex stages very sensitive to input physics. Reaching numerical convergence was not trivial.

Following the encounter, stars exhibit slightly more massive and denser cores alongside a more tenuous envelope, a characteristic that could make them vulnerable to further stripping by either strong winds or interaction with other compact objects. Stripped stars, despite a reduction in mass, maintain a similar radius to their progenitor stars. Their increased brightness, attributed to a larger core, is not significant for distinguishing them from normal stars with equivalent total mass when looking just at an HR diagram. A difference in the evolutionary path between normal and stripped stars is identified in terms of their lifetimes: stripped stars die $\sim 10^6$ years earlier (later) if they are stripped at the final (first) stages of the red giant phase. The difference in lifetimes becomes noteworthy for low-mass stars, such as a $0.7 M_{\odot}$ star, whose natural evolution cannot reach later stages within the age of the universe. The presence of such stars with a substantial helium fraction in their

composition indicates their likely origin as remnants of higher-mass stars that have undergone stripping.

The challenge lies in determining the specific cause of stripping, whether through PTDEs, very strong winds, or other stripping processes. Stripped stars are known in the context of binaries (Li et al., 2022). Further research is essential to find possible unique signatures associated with stars undergoing PTDEs, in order to discriminate from alternative sources of mass loss. The characteristic short dynamical timescale of red giants' core is a key factor in allowing stars to retain a significant portion of their envelopes.

Initially, our research aimed to study the remnants of PTDEs within the context of globular clusters, with the objective of potentially serving as indicators for the presence of intermediate black holes. However, our findings suggest that the identification of such remnants is a challenge, at least through basic observations such as their placement in an HR diagram or even using asteroseismology. It was suggested that more massive stripped stars could be identified due to their unique spectrum (Götberg et al., 2017), but the similarity found between stripped stars and stars with the same total mass suggest that it is unlikely for low and intermediate masses.

Additionally, it is important to consider that stars in globular clusters may undergo stripping not only as a result of interactions with a central black hole but also through interactions with other compact objects, such as neutron stars or white dwarfs.

7 Bibliography

- Angulo, C., Arnould, M., Rayet, M., et al. 1999, Nucl. Phys. A, 656, 3, doi: [10.1016/S0375-9474\(99\)00030-5](https://doi.org/10.1016/S0375-9474(99)00030-5)
- Bloecker, T. 1995, Astronomy and Astrophysics, 297, 727
- Blouin, S., Shaffer, N. R., Saumon, D., & Starrett, C. E. 2020, ApJ, 899, 46, doi: [10.3847/1538-4357/ab9e75](https://doi.org/10.3847/1538-4357/ab9e75)
- Cassisi, S., Potekhin, A. Y., Pietrinferni, A., Catelan, M., & Salaris, M. 2007, ApJ, 661, 1094, doi: [10.1086/516819](https://doi.org/10.1086/516819)
- Chugunov, A. I., Dewitt, H. E., & Yakovlev, D. G. 2007, Phys. Rev. D, 76, 025028, doi: [10.1103/PhysRevD.76.025028](https://doi.org/10.1103/PhysRevD.76.025028)
- Cox, J. P., & Giuli, R. T. 1968, Principles of stellar structure (Cambridge Scientific Publishers)
- Cyburt, R. H., Amthor, A. M., Ferguson, R., et al. 2010, ApJS, 189, 240, doi: [10.1088/0067-0049/189/1/240](https://doi.org/10.1088/0067-0049/189/1/240)
- Ferguson, J. W., Alexander, D. R., Allard, F., et al. 2005, ApJ, 623, 585, doi: [10.1086/428642](https://doi.org/10.1086/428642)
- Frank, J., & Rees, M. J. 1976, Monthly Notices of the Royal Astronomical Society, 176, 633, doi: [10.1093/mnras/176.3.633](https://doi.org/10.1093/mnras/176.3.633)
- Fuller, G. M., Fowler, W. A., & Newman, M. J. 1985, ApJ, 293, 1, doi: [10.1086/163208](https://doi.org/10.1086/163208)

- Götberg, Y., de Mink, S. E., & Groh, J. H. 2017, *Astronomy and Astrophysics*, 608, A11, doi: [10.1051/0004-6361/201730472](https://doi.org/10.1051/0004-6361/201730472)
- Hansen, C. J., Kawaler, S. D., & Trimble, V. 2004, *Stellar Interiors: Physical Principles, Structure, and Evolution*, Astronomy and Astrophysics Library (New York, NY: Springer), doi: [10.1007/978-1-4419-9110-2](https://doi.org/10.1007/978-1-4419-9110-2)
- Heney, L. G., Wilets, L., Böhm, K. H., Lelevier, R., & Levee, R. D. 1959, *ApJ*, 129, 628, doi: [10.1086/146661](https://doi.org/10.1086/146661)
- Herwig, F. 2005, *Annual Review of Astronomy and Astrophysics*, 43, 435, doi: [10.1146/annurev.astro.43.072103.150600](https://doi.org/10.1146/annurev.astro.43.072103.150600)
- Hills, J. G. 1975, *Nature*, 254, 295, doi: [10.1038/254295a0](https://doi.org/10.1038/254295a0)
- Hjellming, M. S., & Webbink, R. F. 1987, *The Astrophysical Journal*, 318, 794, doi: [10.1086/165412](https://doi.org/10.1086/165412)
- Iglesias, C. A., & Rogers, F. J. 1993, *ApJ*, 412, 752, doi: [10.1086/172958](https://doi.org/10.1086/172958)
- . 1996, *ApJ*, 464, 943, doi: [10.1086/177381](https://doi.org/10.1086/177381)
- Irwin, A. W. 2004, *The FreeEOS Code for Calculating the Equation of State for Stellar Interiors*. <http://freeeos.sourceforge.net/>
- Itoh, N., Hayashi, H., Nishikawa, A., & Kohyama, Y. 1996, *ApJS*, 102, 411, doi: [10.1086/192264](https://doi.org/10.1086/192264)
- Jermyn, A. S., Schwab, J., Bauer, E., Timmes, F. X., & Potekhin, A. Y. 2021, *ApJ*, 913, 72, doi: [10.3847/1538-4357/abf48e](https://doi.org/10.3847/1538-4357/abf48e)
- Jermyn, A. S., Bauer, E. B., Schwab, J., et al. 2023, *ApJS*, 265, 15, doi: [10.3847/1538-4365/acae8d](https://doi.org/10.3847/1538-4365/acae8d)
- Kippenhahn, R., Weigert, A., & Weiss, A. 2012, *Stellar Structure and Evolution*, Astronomy and Astrophysics Library (Springer), doi: [10.1007/978-3-642-30304-3](https://doi.org/10.1007/978-3-642-30304-3)

- Langanke, K., & Martínez-Pinedo, G. 2000, Nuclear Physics A, 673, 481, doi: [10.1016/S0375-9474\(00\)00131-7](https://doi.org/10.1016/S0375-9474(00)00131-7)
- Li, Y., Bedding, T. R., Murphy, S. J., et al. 2022, Nature Astronomy, 6, 673, doi: [10.1038/s41550-022-01648-5](https://doi.org/10.1038/s41550-022-01648-5)
- MacLeod, M., Guillochon, J., & Ramirez-Ruiz, E. 2012, The Astrophysical Journal, 757, 134, doi: [10.1088/0004-637X/757/2/134](https://doi.org/10.1088/0004-637X/757/2/134)
- Magorrian, J., & Tremaine, S. 1999, Monthly Notices of the Royal Astronomical Society, 309, 447, doi: [10.1046/j.1365-8711.1999.02853.x](https://doi.org/10.1046/j.1365-8711.1999.02853.x)
- McDonald, I., & Zijlstra, A. 2015, Monthly Notices of the Royal Astronomical Society, 448, 502, doi: [10.1093/mnras/stv007](https://doi.org/10.1093/mnras/stv007)
- Oda, T., Hino, M., Muto, K., Takahara, M., & Sato, K. 1994, Atomic Data and Nuclear Data Tables, 56, 231, doi: [10.1006/adnd.1994.1007](https://doi.org/10.1006/adnd.1994.1007)
- Ostrowski, J., Baran, A. S., Sanjayan, S., & Sahoo, S. K. 2020, Monthly Notices of the Royal Astronomical Society, 503, 4646, doi: [10.1093/mnras/staa3751](https://doi.org/10.1093/mnras/staa3751)
- Passy, J.-C., Herwig, F., & Paxton, B. 2012, The Astrophysical Journal, 760, 90, doi: [10.1088/0004-637X/760/1/90](https://doi.org/10.1088/0004-637X/760/1/90)
- Paxton, B., Bildsten, L., Dotter, A., et al. 2011, ApJS, 192, 3, doi: [10.1088/0067-0049/192/1/3](https://doi.org/10.1088/0067-0049/192/1/3)
- Paxton, B., Cantiello, M., Arras, P., et al. 2013, ApJS, 208, 4, doi: [10.1088/0067-0049/208/1/4](https://doi.org/10.1088/0067-0049/208/1/4)
- Paxton, B., Marchant, P., Schwab, J., et al. 2015, ApJS, 220, 15, doi: [10.1088/0067-0049/220/1/15](https://doi.org/10.1088/0067-0049/220/1/15)
- Paxton, B., Schwab, J., Bauer, E. B., et al. 2018, ApJS, 234, 34, doi: [10.3847/1538-4365/aaa5a8](https://doi.org/10.3847/1538-4365/aaa5a8)

- Paxton, B., Smolec, R., Schwab, J., et al. 2019, *ApJS*, 243, 10, doi: [10.3847/1538-4365/ab2241](https://doi.org/10.3847/1538-4365/ab2241)
- Potekhin, A. Y., & Chabrier, G. 2010, *Contributions to Plasma Physics*, 50, 82, doi: [10.1002/ctpp.201010017](https://doi.org/10.1002/ctpp.201010017)
- Poutanen, J. 2017, *ApJ*, 835, 119, doi: [10.3847/1538-4357/835/2/119](https://doi.org/10.3847/1538-4357/835/2/119)
- Rees, M. J. 1988, *Nature*, 333, 523, doi: [10.1038/333523a0](https://doi.org/10.1038/333523a0)
- Reimers, D. 1975, *Memoires of the Societe Royale des Sciences de Liege*, 8, 369
- Rogers, F. J., & Nayfonov, A. 2002, *ApJ*, 576, 1064, doi: [10.1086/341894](https://doi.org/10.1086/341894)
- Rossi, E. M., Stone, N. C., Law-Smith, J. A. P., et al. 2021, *Space Science Reviews*, 217, 40, doi: [10.1007/s11214-021-00818-7](https://doi.org/10.1007/s11214-021-00818-7)
- Ryu, T., Krolik, J., Piran, T., & Noble, S. C. 2020, *The Astrophysical Journal*, 904, 99, doi: [10.3847/1538-4357/abb3cd](https://doi.org/10.3847/1538-4357/abb3cd)
- Saumon, D., Chabrier, G., & van Horn, H. M. 1995, *ApJS*, 99, 713, doi: [10.1086/192204](https://doi.org/10.1086/192204)
- Stone, N. C., Vasiliev, E., Kesden, M., et al. 2020, *Space Science Reviews*, 216, 35, doi: [10.1007/s11214-020-00651-4](https://doi.org/10.1007/s11214-020-00651-4)
- Syer, D., & Ulmer, A. 1999, *Monthly Notices of the Royal Astronomical Society*, 306, 35, doi: [10.1046/j.1365-8711.1999.02445.x](https://doi.org/10.1046/j.1365-8711.1999.02445.x)
- Timmes, F. X., & Swesty, F. D. 2000, *ApJS*, 126, 501, doi: [10.1086/313304](https://doi.org/10.1086/313304)

A Table of all simulations

Label	Total mass	Core mass	Prog mass	He
100m051c10p025he	1.000	0.515	1.000	0.250
082m052c10p025he	0.816	0.516	1.000	0.250
062m052c10p025he	0.616	0.516	1.000	0.250
100m051c10p050he	1.000	0.506	1.000	0.500
081m051c10p050he	0.806	0.507	1.000	0.500
061m051c10p050he	0.606	0.506	1.000	0.500
100m051c10p075he	1.000	0.493	1.000	0.750
079m049c10p075he	0.793	0.494	1.000	0.750
059m049c10p075he	0.593	0.493	1.000	0.750
150m051c15p025he	1.500	0.526	1.500	0.250
133m053c15p025he	1.326	0.526	1.500	0.250
113m053c15p025he	1.126	0.526	1.500	0.250
093m053c15p025he	0.926	0.526	1.500	0.250
073m053c15p025he	0.726	0.526	1.500	0.250
150m051c15p050he	1.500	0.513	1.500	0.500
131m052c15p050he	1.312	0.515	1.500	0.500
111m051c15p050he	1.112	0.515	1.500	0.500
091m051c15p050he	0.912	0.514	1.500	0.500
071m051c15p050he	0.713	0.513	1.500	0.500
051m051c15p050he	0.513	0.512	1.500	0.500
150m051c15p075he	1.500	0.493	1.500	0.750
129m049c15p075he	1.293	0.494	1.500	0.750
109m049c15p075he	1.093	0.494	1.500	0.750
089m049c15p075he	0.893	0.493	1.500	0.750
069m049c15p075he	0.693	0.493	1.500	0.750

Table A.1: Table of all simulations. Mass is in M_{\odot} units. Labels have the following structure: ###m indicates the total mass, ###c is the core mass, ##p is the progenitor mass and ###he is the helium fraction. All quantities are measured at the time of the stripping, and are expressed in units of M_{\odot} .

Label	Total mass	Core mass	Prog mass	He
200m051c20p025he	2.000	0.531	2.000	0.250
173m053c20p025he	1.731	0.531	2.000	0.250
153m053c20p025he	1.531	0.531	2.000	0.250
133m053c20p025he	1.331	0.531	2.000	0.250
113m053c20p025he	1.131	0.531	2.000	0.250
093m053c20p025he	0.931	0.531	2.000	0.250
073m053c20p025he	0.731	0.531	2.000	0.250
200m051c20p050he	2.000	0.506	2.000	0.500
171m051c20p050he	1.706	0.508	2.000	0.500
151m051c20p050he	1.506	0.507	2.000	0.500
131m051c20p050he	1.306	0.507	2.000	0.500
111m051c20p050he	1.106	0.506	2.000	0.500
091m051c20p050he	0.906	0.506	2.000	0.500
071m051c20p050he	0.706	0.506	2.000	0.500
051m051c20p050he	0.506	0.506	2.000	0.500
200m051c20p075he	2.000	0.475	2.000	0.750
168m048c20p075he	1.675	0.476	2.000	0.750
148m048c20p075he	1.475	0.476	2.000	0.750
127m048c20p075he	1.275	0.475	2.000	0.750
107m048c20p075he	1.075	0.475	2.000	0.750
088m048c20p075he	0.875	0.475	2.000	0.750
068m047c20p075he	0.675	0.475	2.000	0.750

Table A.1: (cont'd) Table of all simulations. Mass is in M_{\odot} units. Labels have the following structure: ###m indicates the total mass, ###c is the core mass, ##p is the progenitor mass and ###he is the helium fraction. All quantities are measured at the time of the stripping, and are expressed in units of M_{\odot} .

Label	Total mass	Core mass	Prog mass	He
300m061c30p025he	3.000	0.674	3.000	0.250
227m067c30p025he	2.274	0.674	3.000	0.250
207m067c30p025he	2.074	0.674	3.000	0.250
187m067c30p025he	1.874	0.674	3.000	0.250
167m067c30p025he	1.674	0.674	3.000	0.250
147m067c30p025he	1.474	0.674	3.000	0.250
127m067c30p025he	1.274	0.674	3.000	0.250
107m067c30p025he	1.074	0.674	3.000	0.250
087m067c30p025he	0.874	0.673	3.000	0.250
067m067c30p025he	0.674	0.672	3.000	0.250
300m061c30p050he	3.000	0.608	3.000	0.500
221m061c30p050he	2.208	0.608	3.000	0.500
201m061c30p050he	2.008	0.608	3.000	0.500
181m061c30p050he	1.808	0.608	3.000	0.500
161m061c30p050he	1.608	0.608	3.000	0.500
141m061c30p050he	1.408	0.608	3.000	0.500
121m061c30p050he	1.208	0.608	3.000	0.500
101m061c30p050he	1.008	0.607	3.000	0.500
081m061c30p050he	0.808	0.607	3.000	0.500
061m061c30p050he	0.608	0.607	3.000	0.500
300m061c30p075he	3.000	0.521	3.000	0.750
212m052c30p075he	2.121	0.522	3.000	0.750
192m052c30p075he	1.921	0.522	3.000	0.750
172m052c30p075he	1.721	0.522	3.000	0.750
152m052c30p075he	1.521	0.522	3.000	0.750
132m052c30p075he	1.321	0.522	3.000	0.750
112m052c30p075he	1.121	0.522	3.000	0.750
092m052c30p075he	0.921	0.522	3.000	0.750
072m052c30p075he	0.721	0.521	3.000	0.750

Table A.1: (cont'd) Table of all simulations. Mass is in M_{\odot} units. Labels have the following structure: ###m indicates the total mass, ###c is the core mass, ##p is the progenitor mass and ###he is the helium fraction. All quantities are measured at the time of the stripping, and are expressed in units of M_{\odot} .

B Figures and tables of Section 5

B.1 Progenitor mass comparison
















Plot #	Color	Label	Total mass	Core mass	Prog mass	He
1		100m051c10p025he	1.000	0.515	1.000	0.250
1		082m052c10p025he	0.816	0.516	1.000	0.250
1		062m052c10p025he	0.616	0.516	1.000	0.250
2		150m051c15p025he	1.500	0.526	1.500	0.250
2		133m053c15p025he	1.326	0.526	1.500	0.250
2		113m053c15p025he	1.126	0.526	1.500	0.250
2		093m053c15p025he	0.926	0.526	1.500	0.250
2		073m053c15p025he	0.726	0.526	1.500	0.250
3		200m051c20p025he	2.000	0.531	2.000	0.250
3		173m053c20p025he	1.731	0.531	2.000	0.250
3		153m053c20p025he	1.531	0.531	2.000	0.250
3		133m053c20p025he	1.331	0.531	2.000	0.250
3		113m053c20p025he	1.131	0.531	2.000	0.250
3		093m053c20p025he	0.931	0.531	2.000	0.250
3		073m053c20p025he	0.731	0.531	2.000	0.250

Table B.1: Legend of figure B.1, which shows the progenitor mass comparison discussed in section 5.2.1










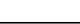



























Plot #	Color	Label	Total mass	Core mass	Prog mass	He
4		300m061c30p025he	3.000	0.674	3.000	0.250
4		227m067c30p025he	2.274	0.674	3.000	0.250
4		207m067c30p025he	2.074	0.674	3.000	0.250
4		187m067c30p025he	1.874	0.674	3.000	0.250
4		167m067c30p025he	1.674	0.674	3.000	0.250
4		147m067c30p025he	1.474	0.674	3.000	0.250
4		127m067c30p025he	1.274	0.674	3.000	0.250
4		107m067c30p025he	1.074	0.674	3.000	0.250
4		087m067c30p025he	0.874	0.673	3.000	0.250
4		067m067c30p025he	0.674	0.672	3.000	0.250
5		100m051c10p050he	1.000	0.506	1.000	0.500
5		081m051c10p050he	0.806	0.507	1.000	0.500
5		061m051c10p050he	0.606	0.506	1.000	0.500
6		150m051c15p050he	1.500	0.513	1.500	0.500
6		131m052c15p050he	1.312	0.515	1.500	0.500
6		111m051c15p050he	1.112	0.515	1.500	0.500
6		091m051c15p050he	0.912	0.514	1.500	0.500
6		071m051c15p050he	0.713	0.513	1.500	0.500
6		051m051c15p050he	0.513	0.512	1.500	0.500
7		200m051c20p050he	2.000	0.506	2.000	0.500
7		171m051c20p050he	1.706	0.508	2.000	0.500
7		151m051c20p050he	1.506	0.507	2.000	0.500
7		131m051c20p050he	1.306	0.507	2.000	0.500
7		111m051c20p050he	1.106	0.506	2.000	0.500
7		091m051c20p050he	0.906	0.506	2.000	0.500
7		071m051c20p050he	0.706	0.506	2.000	0.500
7		051m051c20p050he	0.506	0.506	2.000	0.500
8		300m061c30p050he	3.000	0.608	3.000	0.500
8		221m061c30p050he	2.208	0.608	3.000	0.500
8		201m061c30p050he	2.008	0.608	3.000	0.500
8		181m061c30p050he	1.808	0.608	3.000	0.500
8		161m061c30p050he	1.608	0.608	3.000	0.500
8		141m061c30p050he	1.408	0.608	3.000	0.500
8		121m061c30p050he	1.208	0.608	3.000	0.500
8		101m061c30p050he	1.008	0.607	3.000	0.500
8		081m061c30p050he	0.808	0.607	3.000	0.500
8		061m061c30p050he	0.608	0.607	3.000	0.500

Table B.1: (cont'd) Legend of figure B.1, which shows the progenitor mass comparison discussed in section 5.2.1

























Plot #	Color	Label	Total mass	Core mass	Prog mass	He
9		100m051c10p075he	1.000	0.493	1.000	0.750
9		079m049c10p075he	0.793	0.494	1.000	0.750
9		059m049c10p075he	0.593	0.493	1.000	0.750
10		150m051c15p075he	1.500	0.493	1.500	0.750
10		129m049c15p075he	1.293	0.494	1.500	0.750
10		109m049c15p075he	1.093	0.494	1.500	0.750
10		089m049c15p075he	0.893	0.493	1.500	0.750
10		069m049c15p075he	0.693	0.493	1.500	0.750
11		200m051c20p075he	2.000	0.475	2.000	0.750
11		168m048c20p075he	1.675	0.476	2.000	0.750
11		148m048c20p075he	1.475	0.476	2.000	0.750
11		127m048c20p075he	1.275	0.475	2.000	0.750
11		107m048c20p075he	1.075	0.475	2.000	0.750
11		088m048c20p075he	0.875	0.475	2.000	0.750
11		068m047c20p075he	0.675	0.475	2.000	0.750
12		300m061c30p075he	3.000	0.521	3.000	0.750
12		212m052c30p075he	2.121	0.522	3.000	0.750
12		192m052c30p075he	1.921	0.522	3.000	0.750
12		172m052c30p075he	1.721	0.522	3.000	0.750
12		152m052c30p075he	1.521	0.522	3.000	0.750
12		132m052c30p075he	1.321	0.522	3.000	0.750
12		112m052c30p075he	1.121	0.522	3.000	0.750
12		092m052c30p075he	0.921	0.522	3.000	0.750
12		072m052c30p075he	0.721	0.521	3.000	0.750

Table B.1: (cont'd) Legend of figure B.1, which shows the progenitor mass comparison discussed in section 5.2.1

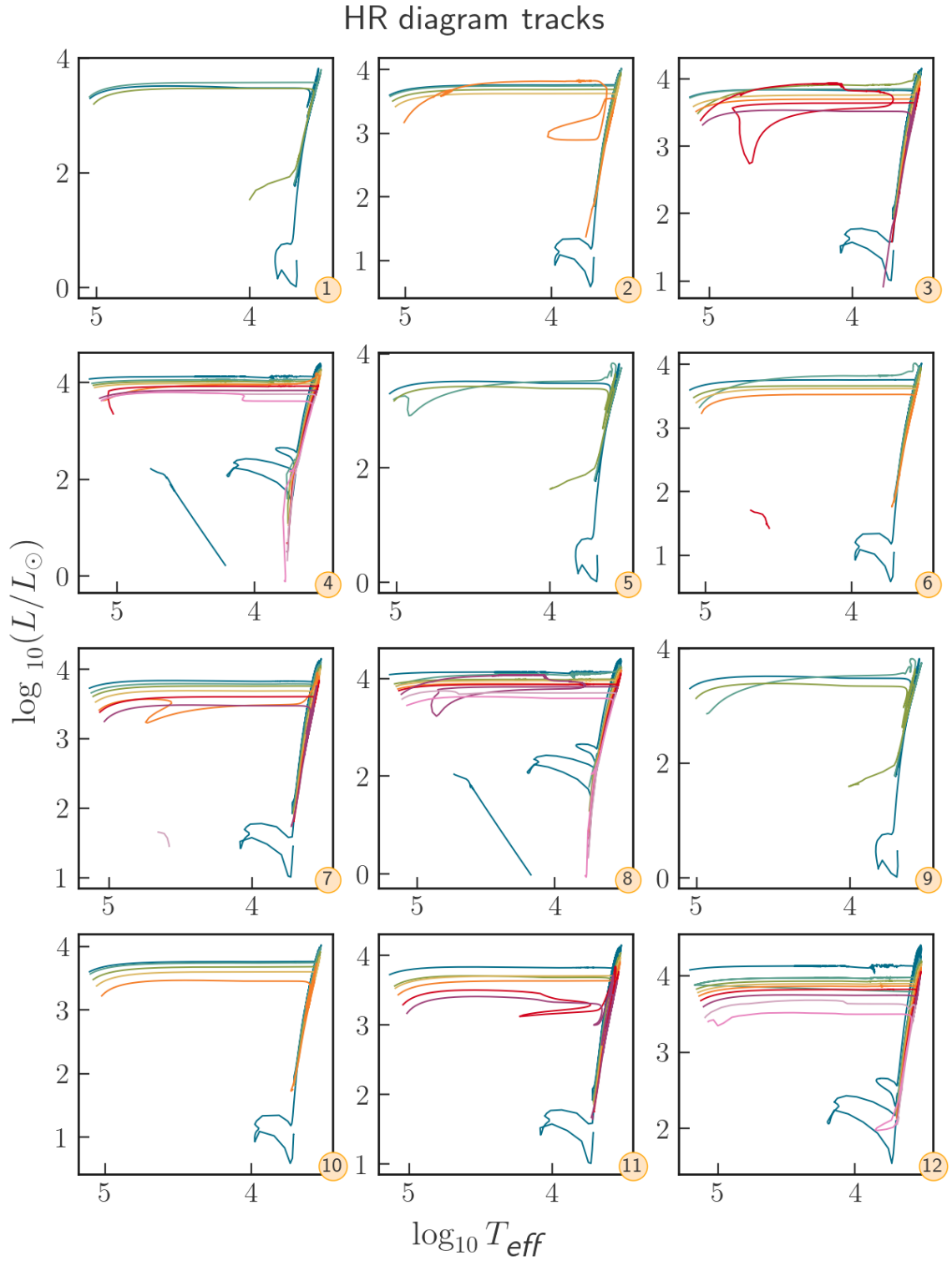


Figure B.1: HR diagram tracks for same progenitor mass, in order to compare the progenitor normal stars with the stripped stars. Legend can be seen in table B.1

B.2 Total mass comparison






























Plot #	Color	Label	Total mass	Core mass	Prog mass	He
1		073m053c20p025he	0.731	0.531	2.000	0.250
1		073m053c15p025he	0.726	0.526	1.500	0.250
1		067m067c30p025he	0.674	0.672	3.000	0.250
1		062m052c10p025he	0.616	0.516	1.000	0.250
2		107m067c30p025he	1.074	0.674	3.000	0.250
2		100m051c10p025he	1.000	0.515	1.000	0.250
2		093m053c20p025he	0.931	0.531	2.000	0.250
2		093m053c15p025he	0.926	0.526	1.500	0.250
3		127m067c30p025he	1.274	0.674	3.000	0.250
3		113m053c20p025he	1.131	0.531	2.000	0.250
3		113m053c15p025he	1.126	0.526	1.500	0.250
4		153m053c20p025he	1.531	0.531	2.000	0.250
4		150m051c15p025he	1.500	0.526	1.500	0.250
4		147m067c30p025he	1.474	0.674	3.000	0.250
5		187m067c30p025he	1.874	0.674	3.000	0.250
5		173m053c20p025he	1.731	0.531	2.000	0.250
6		207m067c30p025he	2.074	0.674	3.000	0.250
6		200m051c20p025he	2.000	0.531	2.000	0.250
7		071m051c15p050he	0.713	0.513	1.500	0.500
7		071m051c20p050he	0.706	0.506	2.000	0.500
7		061m061c30p050he	0.608	0.607	3.000	0.500
7		061m051c10p050he	0.606	0.506	1.000	0.500
8		101m061c30p050he	1.008	0.607	3.000	0.500
8		100m051c10p050he	1.000	0.506	1.000	0.500
8		091m051c15p050he	0.912	0.514	1.500	0.500
8		091m051c20p050he	0.906	0.506	2.000	0.500
9		121m061c30p050he	1.208	0.608	3.000	0.500
9		111m051c15p050he	1.112	0.515	1.500	0.500
9		111m051c20p050he	1.106	0.506	2.000	0.500

Table B.2: Legend of figure B.2, which shows the progenitor mass comparison discussed in section 5.2.2
























Plot #	Color	Label	Total mass	Core mass	Prog mass	He
10		151m051c20p050he	1.506	0.507	2.000	0.500
10		150m051c15p050he	1.500	0.513	1.500	0.500
10		141m061c30p050he	1.408	0.608	3.000	0.500
11		181m061c30p050he	1.808	0.608	3.000	0.500
11		171m051c20p050he	1.706	0.508	2.000	0.500
12		201m061c30p050he	2.008	0.608	3.000	0.500
12		200m051c20p050he	2.000	0.506	2.000	0.500
13		079m049c10p075he	0.793	0.494	1.000	0.750
13		072m052c30p075he	0.721	0.521	3.000	0.750
13		069m049c15p075he	0.693	0.493	1.500	0.750
13		068m047c20p075he	0.675	0.475	2.000	0.750
14		109m049c15p075he	1.093	0.494	1.500	0.750
14		107m048c20p075he	1.075	0.475	2.000	0.750
14		100m051c10p075he	1.000	0.493	1.000	0.750
14		092m052c30p075he	0.921	0.522	3.000	0.750
15		129m049c15p075he	1.293	0.494	1.500	0.750
15		127m048c20p075he	1.275	0.475	2.000	0.750
15		112m052c30p075he	1.121	0.522	3.000	0.750
16		152m052c30p075he	1.521	0.522	3.000	0.750
16		150m051c15p075he	1.500	0.493	1.500	0.750
16		148m048c20p075he	1.475	0.476	2.000	0.750
17		200m051c20p075he	2.000	0.475	2.000	0.750
17		192m052c30p075he	1.921	0.522	3.000	0.750

Table B.2: (cont'd) Legend of figure B.2, which shows the total mass comparison discussed in section 5.2.2.

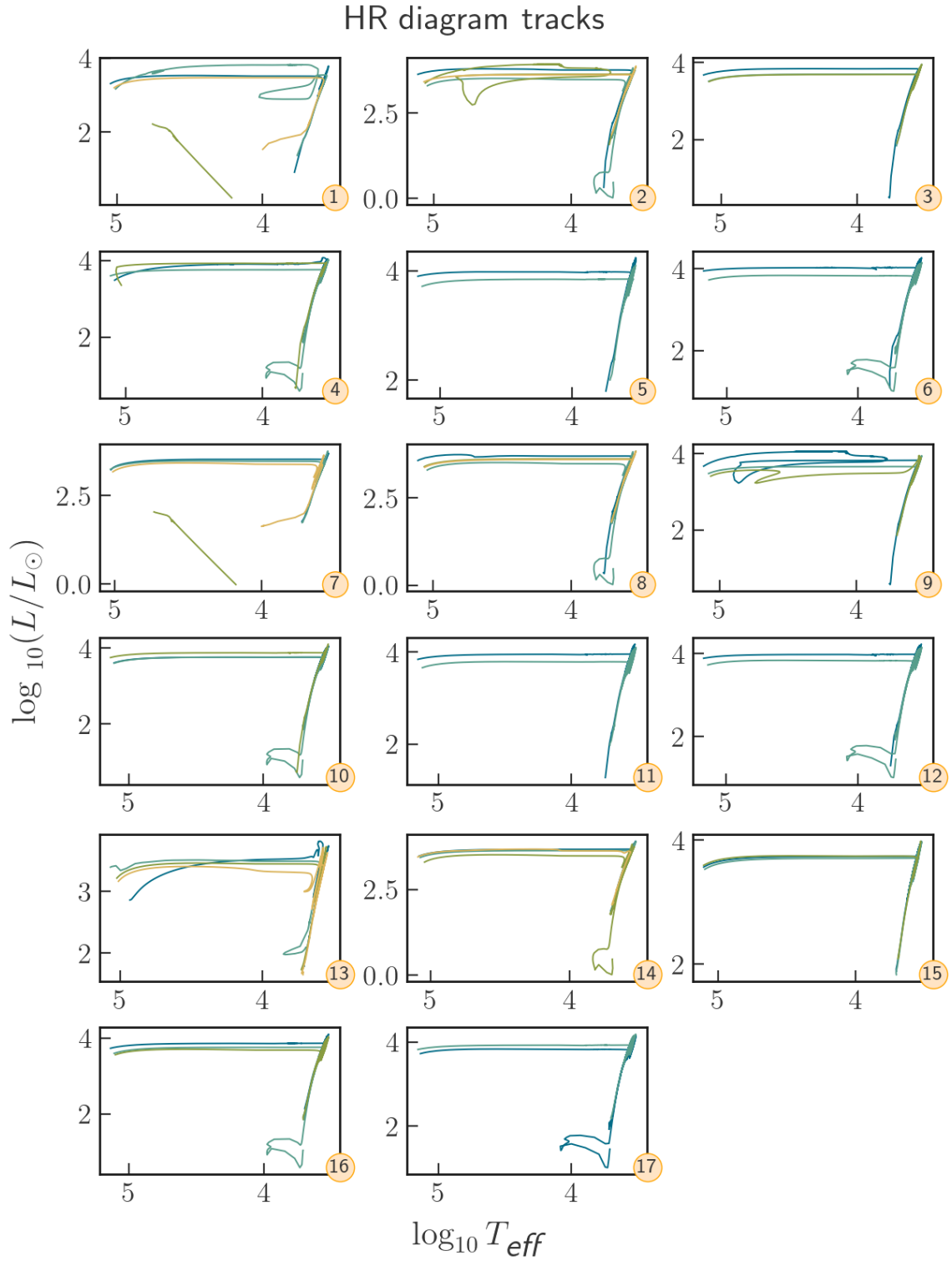


Figure B.2: HR diagram tracks for same total mass, in order to compare the normal stars with stripped stars. Legend can be seen in table B.2

B.3 Stripping time comparison


























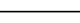
Plot #	Color	Label	Total mass	Core mass	Prog mass	He
1		079m049c10p075he	0.793	0.494	1.000	0.750
1		062m052c10p025he	0.616	0.516	1.000	0.250
1		061m051c10p050he	0.606	0.506	1.000	0.500
2		073m053c15p025he	0.726	0.526	1.500	0.250
2		071m051c15p050he	0.713	0.513	1.500	0.500
2		069m049c15p075he	0.693	0.493	1.500	0.750
3		109m049c15p075he	1.093	0.494	1.500	0.750
3		093m053c15p025he	0.926	0.526	1.500	0.250
3		091m051c15p050he	0.912	0.514	1.500	0.500
4		129m049c15p075he	1.293	0.494	1.500	0.750
4		113m053c15p025he	1.126	0.526	1.500	0.250
4		111m051c15p050he	1.112	0.515	1.500	0.500
5		073m053c20p025he	0.731	0.531	2.000	0.250
5		071m051c20p050he	0.706	0.506	2.000	0.500
5		068m047c20p075he	0.675	0.475	2.000	0.750
6		107m048c20p075he	1.075	0.475	2.000	0.750
6		093m053c20p025he	0.931	0.531	2.000	0.250
6		091m051c20p050he	0.906	0.506	2.000	0.500
7		127m048c20p075he	1.275	0.475	2.000	0.750
7		113m053c20p025he	1.131	0.531	2.000	0.250
7		111m051c20p050he	1.106	0.506	2.000	0.500
8		153m053c20p025he	1.531	0.531	2.000	0.250
8		151m051c20p050he	1.506	0.507	2.000	0.500
8		148m048c20p075he	1.475	0.476	2.000	0.750
9		173m053c20p025he	1.731	0.531	2.000	0.250
9		171m051c20p050he	1.706	0.508	2.000	0.500

Table B.3: Legend of figure B.3, which shows the stripping time comparison discussed in section 5.2.3



















Plot #	Color	Label	Total mass	Core mass	Prog mass	He
10		072m052c30p075he	0.721	0.521	3.000	0.750
10		067m067c30p025he	0.674	0.672	3.000	0.250
10		061m061c30p050he	0.608	0.607	3.000	0.500
11		107m067c30p025he	1.074	0.674	3.000	0.250
11		101m061c30p050he	1.008	0.607	3.000	0.500
11		092m052c30p075he	0.921	0.522	3.000	0.750
12		127m067c30p025he	1.274	0.674	3.000	0.250
12		121m061c30p050he	1.208	0.608	3.000	0.500
12		112m052c30p075he	1.121	0.522	3.000	0.750
13		152m052c30p075he	1.521	0.522	3.000	0.750
13		147m067c30p025he	1.474	0.674	3.000	0.250
13		141m061c30p050he	1.408	0.608	3.000	0.500
14		187m067c30p025he	1.874	0.674	3.000	0.250
14		181m061c30p050he	1.808	0.608	3.000	0.500
14		172m052c30p075he	1.721	0.522	3.000	0.750
15		207m067c30p025he	2.074	0.674	3.000	0.250
15		201m061c30p050he	2.008	0.608	3.000	0.500
15		192m052c30p075he	1.921	0.522	3.000	0.750

Table B.3: (cont'd) Legend of figure B.3, which shows the stripping time comparison discussed in section 5.2.3

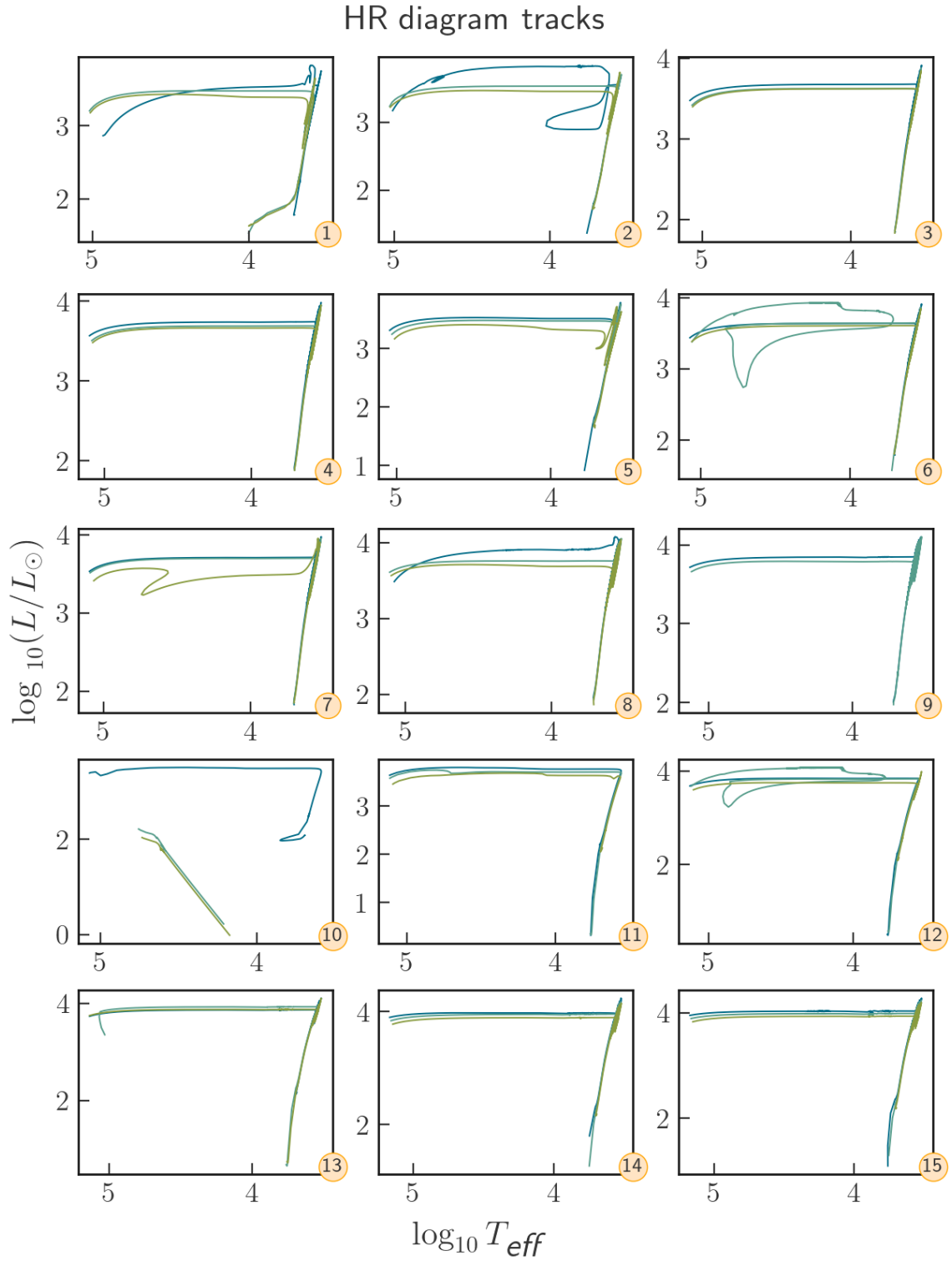


Figure B.3: HR diagram tracks for same progenitor mass stars and same total mass, in order to compare the effect of stripping at different helium fractions. Legend can be seen in table B.3.